BioRT-HBV 1.0: a Biogeochemical Reactive Transport Model at the Watershed Scale

Kayalvizhi Sadayappan[1], Bryn Stewart[1], Devon Kerins[1], Andrew Vierbicher[1], Wei Zhi[1], Marc Vis[2], Jan Seibert[2], Li Li[1,*]

[1] Department of Civil and Environmental Engineering, The Pennsylvania State University, University Park, PA, USA

[2] Department of Geography, University of Zurich, Zurich, Switzerland

*Corresponding author: lili@engr.psu.edu

Key Points:

- We introduce BioRT-HBV, a watershed scale reactive transport model that is parsimonious, flexible, easy to use and requires minimal data
- BioRT-HBV can simulate a variety of user-defined biogeochemical processes, including carbon and nitrogen processes
- BioRT-HBV is open source for any researchers interested in ecohydrological and biogeochemical processes

Abstract

Reactive Transport Models (RTMs) are essential for understanding and predicting intertwined ecohydrological and biogeochemical processes on land and in rivers. While traditional RTMs have focused primarily on subsurface processes, recent RTMs integrate hydrological and biogeochemical interactions between land surface and subsurface. These emergent, watershed-scale RTMs are often spatially explicit and require large amount of data and extensive computational expertise. There is however a pressing need to create parsimonious models that require less data and are accessible to scientists with less computational background. Here we introduce BioRT-HBV 1.0 (hereafter BioRT), a watershed-scale, hydro-biogeochemical model that builds upon the widely used, bucket-type HBV model (Hydrologiska Bryåns Vattenavdelning), known for its simplicity and minimal data requirements. BioRT uses the conceptual structure and

hydrology output of HBV to simulate processes including solute transport and biogeochemical reactions driven by reaction thermodynamics and kinetics. These reactions include, for example, chemical weathering, soil respiration, and nutrient transformation. This paper presents the model structure and governing equations, demonstrates its utility with examples simulating carbon and nitrogen processes in a headwater catchment. As shown in the examples, when constrained by data, BioRT can be used to illuminate the dynamics of biogeochemical reactions in the invisible, arduous-to-measure subsurface, and their connections to observed solute export in streams and rivers. We posit that such parsimonious models increase model accessibility to users without in-depth computational training. It also can serve as an educational tool that promote pollination of ideas across different fields and foster a more diverse, equal, and inclusive user community.

Plain Language Summary

Reactive Transport models (RTMs) are essential tools to understand the movement of water, nutrients and other elements from land to rivers and their interactions with each other. Recent RTMs at the watershed scale, unlike earlier ones that primarily focus on subsurface processes, have integrated belowground processes and above-ground dynamics and characteristics including changing weather and vegetation cover. However, these models require large amount of data and are challenging for users from diverse backgrounds, including those with limited computational background. Here we introduce BioRT-HBV 1.0 (hereafter BioRT), a parsimonious, watershed-scale RTM that is relatively easy to learn and use and requires minimal data. BioRT can simulate a wide variety of processes like chemical weathering, carbon and nutrient transformation, soil organic carbon decomposition, among others. Here, we introduce the model structure, governing equations, and examples that illustrate the use of model in simulating carbon and nitrogen processes. We put forward this model as a potential research and educational tool that can be used by students and researchers from diverse disciplines.

1. INTRODUCTION

Hydrological and biogeochemical processes at the watershed scale collectively shape the timing, magnitude, and quality of stream water. These processes include water flow and partitioning, and biogeochemical transformation and transport. They are driven by external hydroclimatic forcings and human perturbations, while modulated by watershed characteristics including soil structure, lithology, vegetation cover, land use, and topography (Li et al., 2022; Li et al., 2021; McDowell et al., 2023; Sullivan et al., 2022). It is essential to understand interacting hydrological and biogeochemical processes and to forecast river water response to future climate and human perturbations (Li, 2019).

Water quality models have been developed for these purposes. Examples include SWAT (Soil Water Assessment Tool) (Hu et al., 2007; Luo & Zhang, 2009; Rajib et al., 2020), HSPF (Hydrological Simulation Program – FORTRAN) (Filoso et al., 2004; Laroche et al., 1996), HYPE (Hydrological Predictions for the Environment) (Arheimer et al., 2012; Veinbergs et al., 2017), MIKE SHE (Système Hydrologique Européen) (Hou et al., 2021; Jaber & Shukla, 2012), and INCA (INtegrated CAtchment model) (Bastrup-Birk & Gundersen, 2004; Wade et al., 2002). Most of these existing water quality models focus on a limited number of defined reactions and solutes a priori and have limited flexibility of modifying included reactions. As an example, the PULSE model – the first water quality model based on HBV (Hydrologiska Bryåns Vattenavdelning) – simulates variations in stream pH and alkalinity (Bergström et al., 1985). The PULSE model was later augmented to simulate the transport of the conservative tracer ^{18}O (Lindström & Rodhe, 1986) and inorganic nitrogen (Bergström et al., 1987; Brandt, 1990). Nitrogen (N) processes were further expanded to consider nitrogen transformation in streams, lakes and wetlands, ultimately leading to the development of the HBV-N model (Arheimer & Brandt, 1998; Arheimer & Wittgren, 1994; Pettersson et al., 2001). This model evolved into HBV-NP that includes transport and transformation of soluble and particulate phosphorus (P) (Andersson et al., 2005; Arheimer et al., 2005). Based on HBV-NP, the Hydrological Predictions for the Environment (HYPE) model was developed for simulations at high spatial resolution (Lindström et al., 2010).

The HYPE model has been further modified to add organic carbon processes (Pers et al., 2016). The model can now simulate carbon and nutrient processes but lacks the capability to model other solutes such as cations and anions from chemical weathering.

Biogeochemical reactions are complex and often cover a wide range of solutes and processes, varying from abiotic reactions such as chemical weathering to biotic reactions such as soil respiration, nutrient transformation, and plant uptake of nutrients. Users often do not know which reactions play a predominant role for particular nutrient or solute dynamics a priori. There is a need for generic, flexible models where users can define the types of reactions and solutes such that different types of reactions can be tested. Multi-component Reactive Transport Models (RTMs) can serve this purpose. These models solve reactive transport equations for a variety of user-defined solutes based on reaction stoichiometry and thermodynamics and kinetics defined in a generic database and input files (Steefel et al., 2015; Steefel & MacQuarrie, 1996). Traditional RTMs have primarily focused on subsurface processes (Li, Maher, et al., 2017; Lichtner, 1988). Recent RTMs have evolved to include land surface processes and their interactions with subsurface processes at the watershed scale (Bao et al., 2017; Jan et al., 2021; Zhi et al., 2022).

The emergent watershed-scale RTMs have facilitated our understanding of complex hydrological and biogeochemical coupling. However, characterized by spatial and computational complexity, these models require intensive measurements that are often only available in intensively monitored catchments. The computational complexity also limits the models to be accessible mostly to users with extensive computational background. There is a pressing need for flexible and parsimonious models that are accessible to users without extensive computational training.

In this context, we developed BioRT-HBV model that integrates the widely-used hydrologic model HBV with BioRT, the biogeochemical module of BioRT-Flux-PIHM (Zhi et al., 2022). HBV is a semi-distributed, bucket-type hydrological model that has been used to simulate watershed-scale hydrological processes in more than 30 countries (Bergström, 1992; Seibert & Bergström, 2022). It has also been used widely for educational purposes to teach hydrology concepts (Seibert & Vis, 2012). It originated in

the 1970s (Bergström, 1992; Bergström & Forsman, 1973) and now has several different versions for different purposes (Bergström & Lindström, 2015). The driving philosophy of HBV has been a simple but robust model with minimal data requirements (Lindström et al., 1997). The HBV-light version offers a user-friendly graphical user interface and has been widely used for both educational and research purposes (Seibert & Vis, 2012).

BioRT uses the hydrological output from HBV-light, including soil moisture, water storage, and flow. BioRT follows the development of traditional reactive transport approaches widely used in the geochemistry community (Lichtner, 1988; Steefel et al., 2015; Steefel & MacQuarrie, 1996). BioRT can model a variety of biogeochemical processes including chemical weathering and soil respiration, nutrient transformation, and sediment mobilization. The reactive transport code is written generically to allow users to define the system of reactions and solutes and solids they intend to simulate in input files. Its extensive database defines reaction stoichiometry, thermodynamics, and kinetics, and can be extended by users. Here we present the model description, governing equations, and numerical scheme. We additionally show example applications in simulating reactive transport processes at the watershed scale in Sleepers River, Vermont, USA.

2. MODEL DESCRIPTION

2.1 Model structure

The “standard” HBV model has been well documented in literature (Bergström, 1992; Seibert & Vis, 2012). Here we briefly describe the model structure of HBV that is necessary to understand the structure of BioRT-HBV. HBV-light simulates hydrological processes, including evapotranspiration and streamflow generation, and partitions streamflow into three major lateral flow paths, Q_0, Q_1, and Q_2, that drain into rivers and streams. The model includes two subsurface zones, the upper and lower zones (UZ and LZ), which we conceptually consider as corresponding to the shallow soil zone (SZ) and deeper groundwater zone (DZ) in BioRT, respectively (Figure 1). The shallow zone represents the subsurface where transient lateral water flow can form or where the water table can rise to under very wet conditions (Sullivan et al., 2016; Torres et al.,

2015). This is the zone where water comes and goes quickly and interacts with weathered minerals and organic matter in soil. The deep zone represents the deeper subsurface that is generally saturated and provides baseflow under low flow conditions. Conceptually this can represent shallow aquifers below the soil zone where older water is in contact with partially weathered or parent bedrock (Anderson et al., 1997; Frisbee et al., 2013).

An additional surface zone (SF) was added in BioRT to represent the transient above-ground water storage. As rainfall arrives and snowmelt occurs at the ground surface, water can either infiltrate to the subsurface or flow directly to the stream as surface runoff. While infiltrating water chemistry may depend only on the mixing of snowmelt water and rainfall, surface runoff can interact with the ground surface and top subsurface layers such as surface organic matter and litter, and mobilize fine sediments (soil erosion), ashes, road salts and nutrients on its way towards streams. These reactions influence the chemistry of the surface runoff reaching the stream though not the infiltrating water, and can be simulated in surface zone. Each zone is considered as a well-mixed reactor in the model.

HBV-light calculates the soil moisture and “dynamic” water storage in upper and lower zone that generates streamflow. Some water in subsurface does not contribute to streamflow generation but participate in evapotranspiration, solute transport, and reactions. This “passive” water storage is not modelled by HBV, and we assign these values for shallow and deep zones in BioRT input files. The signature of this storage is often reflected in tracer transport and stream chemistry and therefore can be calibrated using tracer and stream chemistry data.

To assign physical meanings to the three flows, we slightly changed the HBV terminology in BioRT (Figure 1). We use Q_{SF} for Q_0, conceptually representing rapid surface flow or quick flow; Q_{SZ} for Q_1, representing lateral flow from the shallow soil zone; and Q_{DZ} for Q_2, representing flow from the deep groundwater zone. The sum of the three flows is the total stream discharge (Q). The relative contributions of these three flows to discharge depend on hydroclimate forcings and the land and subsurface characteristics. They are quantified by calibrating model parameters in HBV that

characterize how water moves through a watershed, including, for example, how much water infiltrates to the shallow zone and recharges (or percolates according to the typical HBV language) to the deep zone to become deeper groundwater. Note that these three flows are simplified representations of innumerable flow paths in natural systems. Such simplification is necessary as we do not have the data and computational luxury to fully represent these details.

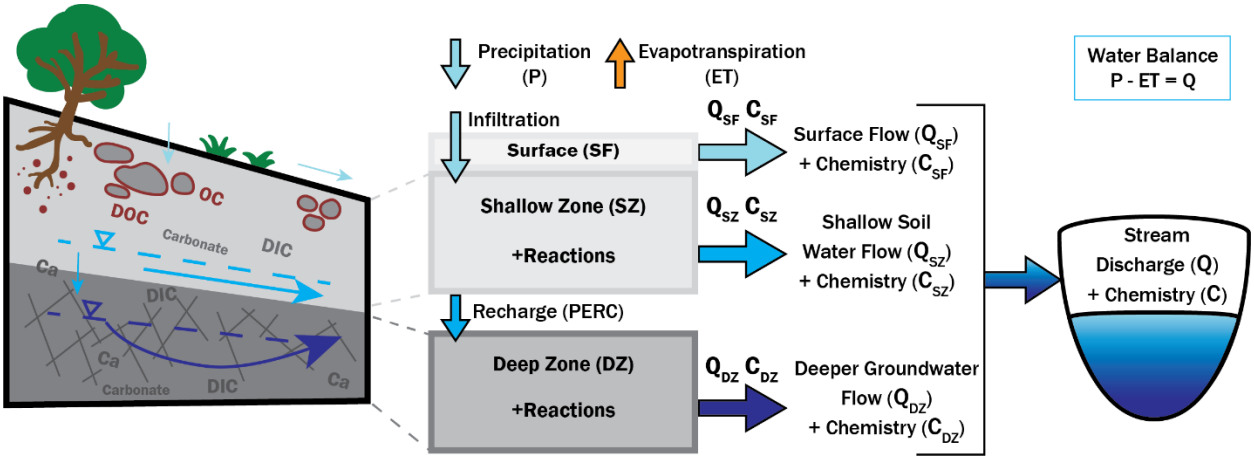

***Figure 1**: A conceptual diagram of BioRT-HBV model structure. Note that the shallow zone (SZ) and deep zone (DZ) correspond to upper and lower zones in HBV-light, such that Q_{SF}, Q_{SZ}, and Q_{DZ} correspond to the flows defined in HBV-light as Q_0, Q_1, and Q_2, respectively. BioRT has an additional surface zone (SF) for potential reactions that mobilize solutes and solids at the ground surface. The BioRT model can incorporate input precipitation chemistry and user-defined reaction networks in the SF, SZ and DZ, such that distinct biogeochemical processes can be simulated in each zone for each flow path that contributes to the stream.*

2.2 Governing equations

In multi-component reactive transport systems, we have multiple solute species participating in multiple reactions. Following RTM tradition (Lichtner, 1988; Steefel & MacQuarrie, 1996), BioRT solves the governing equations for each zone for the primary species. The primary species are the building blocks of the chemical system; the secondary species can be expressed by the concentrations of primary species via equilibrium reactions and laws of mass action. This approach eliminates the need to solve for all species via time stepping. The model solves differential equations only for the concentrations of primary species, based on which the concentrations of secondary species can be calculated. Here we write the equations for an arbitrary primary species *i* within a total number of *n* primary species.

In the surface zone (SF):

$$\frac{dC_{SF,i}V_{w,SF}}{dt} = P_{rain}C_{rain,i} + Q_{snowmelt}C_{snowmelt,i} - Q_{SF}C_{SF,i} - Q_{infil}C_{infil,i} + R_{SF},\ i = 1, \dots, n \quad (1)$$

where the solute concentration in the infiltrating water $C_{infil,i}$ is determined by the mixing of rainwater and snowmelt water: $C_{infil,i} = \frac{P_{rain}C_{rain,i} + Q_{snowmelt}C_{snowmelt,i}}{P_{rain} + Q_{snowmelt,i}}$. Snow can accumulate at the ground surface, and is kept track using the equation: $\frac{dC_{snow,i}V_{snow}}{dt} = P_{snow}C_{ppt,i} - Q_{snowmelt}C_{snow,i}$

In the Shallow Zone (SZ):

$$\frac{d(C_{SZ,i}V_{w,SZ})}{dt} = Q_{infil}C_{infil,i} - \left(Q_{SZ} + Q_{perc}\right)C_{SZ,i} + R_{SZ,i}, = 1, \dots, n \quad (2)$$

In the Deep Zone (DZ):

$$\frac{d(C_{DZ,i}V_{w,DZ})}{dt} = Q_{perc}C_{SZ,i} - Q_{DZ}C_{DZ,i} + R_{DZ,i,} \quad i, = 1, \dots, n \quad (3)$$

where P_{snow} is the precipitation falling as snow, P_{rain} is the precipitation falling as rainfall, $Q_{snowmelt}$ is the flow from snowmelt, Q_{infil} is the infiltrating water flow entering the shallow zone, Q_{perc} is the water percolating (or recharge) from shallow to deep zone. Here $V_{w,SF}$, $V_{w,SZ}$, and $V_{w,DZ}$ are the water storage in surface zone, shallow zone, and deep zone, respectively, and $V_{w,snow}$ is the water storage in the snow. The $C_{ppt,i}$, $C_{snow,i}$, $C_{infil,i}$, $C_{SF,i}$, $C_{SZ,i,}$ and $C_{DZ,i}$ are concentrations of solute i in precipitation, snow, infiltrating water entering shallow zone, surface zone, shallow zone, and deep zone, respectively. The reaction rates $R_{SF,i}$, $R_{SZ,i}$, and $R_{DZ,i}$ are those of solute i in surface zone, shallow zone, and deep zone, respectively. If a solute participates in more than one reaction, the rates of each reaction can be spelled out separately and each R term is the summation of multiple reaction rates in each zone, as exemplified later in the example applications. Water volume (V) and water fluxes (Q) are drainage-area-normalized values and have units of mm (volume per unit drainage area) and mm/time of water respectively. Concentrations (C) and reaction rates (R) are in the unit of mole/l and mole/l/time respectively.

2.3 Reactions

BioRT can simulate a variety of reactions including chemical weathering (e.g., mineral dissolution and precipitation), microbial and root respiration reactions, nutrient transformation, ion exchange, surface complexation, among others. Users can define the types of reactions and solutes to be included in the reaction network, and the form of reaction rate laws.

2.3.1 Rate laws of weathering reactions

For weathering reactions, the rates generally follow the classic Transition State Theory (TST) (Aagaard & Helgeson, 1982; Helgeson et al., 1984; Lasaga, 1984), which prescribes reaction rates as dependent on mineral properties, concentrations of some catalyzing solutes, and how far away the reaction is from equilibrium:

$$r = A_{mineral} k a^m \left(1 - \frac{IAP}{K_{eq}}\right) \quad (4)$$

Here r is the reaction rate (mol/m^3/time), $A_{mineral}$ is the mineral surface area per unit volume (m^2/m^3), k is the kinetic reaction rate constant of the reaction (mol/m^2/time), K_{eq} is the equilibrium constant of the reaction, 'a' represents the activity (equals to concentration in most natural inland waters) of a solute that can catalyze or inhibit weathering, and the exponent 'm' describes the extent of dependence on the solute. For example, hydrogen ion (H^+) often accelerates weathering such that the reaction rates depend on pH. The ratio IAP (Ion Activity Product) / K_{eq} describes how far away the reaction is from equilibrium;

2.3.2 Rates of biologically mediated reactions

It is well known that rates of reactions such as soil respiration and nutrient transformation in natural subsurface generally depend on conditions including temperature, soil moisture, and water table level (Davidson et al., 2004; Davidson & Janssens, 2006). As such, reaction rates depend not only on properties of reacting mineral or substrate, but also on these conditions. We therefore use a rate law with dependence functions in BioRT to account for these effects:

$$r = kA\, f(T) f(S_w) f(Z_w) \quad (5)$$

Here r is the reaction rate (mol/m^3/time), k is the reaction rate constant (mol/m^3/time), A is the material surface area abundance (m^2/m^3); and f(T), f(S_w), and f(Z_w) describe the rate dependence on temperature (T), soil moisture (S_w), and water table levels (Z_w), respectively, as detailed below.

Temperature dependence function f(T): Biotic reaction rates typically increase with temperature. Here we use the Q_{10}-based approach that has been widely adopted (Davidson & Janssens, 2006; Elberling, 2005).

$$f(T) = Q_{10}^{|T-20|/10} \quad (6)$$

where Q_{10} is the temperature coefficient representing relative increase in rates when temperature increases by 10°Celsius, and T is temperature (°C). If Q_{10} is 1, f(T) becomes 1 such that the rate has no dependence on temperature.

Soil moisture dependence function f(S_w): Microbial respiration rates typically increase with soil moisture until some intermediate value, beyond which the rates decrease as they change from substrate limited to oxygen limited (Or et al., 2007). Similarly, root respiration rates also peak at some intermediate soil moisture conditions. To model dependence on soil moisture, BioRT uses the following generic dependence function (Yan et al., 2018):

$$f(S_w) = \begin{cases} \left(\frac{S_w}{S_{w,c}}\right)^n, \text{when } S_w < S_{w,c} \\ \left(\frac{1-S_w}{1-S_{w,c}}\right)^n, \text{when } S_w > S_{w,c} \end{cases} \quad (7)$$

where S_w is the soil moisture, $S_{w,c}$ is the critical soil moisture at which reaction rate peaks, and n is soil moisture dependence exponent. The term $S_{w,c}$ indicates that increasing moisture content does not always translate to higher rates. For example, under water-saturated conditions, O_2 becomes limited such that the relatively fast aerobic reactions slow down and generally slower anaerobic reactions become dominant, which reduce the overall rates of biogeochemical reactions (Schlesinger & Bernhardt, 2020). Under rare conditions where rates do not depend on soil moisture, n can be set as zero to disable the soil moisture dependence. This function can also be used for abiotic weathering reactions. Weathering rates typically increase with water

content as increasing soil moisture wet mineral surface area (Li, Bao, et al., 2017). This means that the $S_{w,c}$ for weathering reactions are one or close to one such that $f(S_w)$ almost always increase with water content.

Water table depth dependence function $f(Z_w)$: In addition to soil moisture, water table depth and the depth distribution of solute sources can further influence reaction rates and solute mobilization (Seibert et al., 2009; Zhi & Li, 2020). For example, organic matter is typically more abundant at shallow depths (Souza et al., 2023) such that shallow water tables can often access more organic matter and mobilize dissolved organic carbon (DOC) that is sorbed on soil surface to stream. A rising water table can also promote lateral and vertical hydrological connectivity and enhance reaction rates (Clow & Mast, 2010; Xiao et al., 2021). On the other hand, falling water table in peat lands have been associated with elevated soil respiration and carbon losses (L. Ma et al., 2022). BioRT uses an exponential function to account for the water table depth dependence following practices in literature (Bai et al., 2016; Ottoy et al., 2016; Seibert et al., 2009).

$$f(Z_w) = exp\left(-\alpha {Z_w}^{\beta}\right) \quad (8)$$

where Z_w is water table depth, α and β are parameters that determine the magnitude and direction of the dependence on water table depth respectively. When α = 0, the rates have no dependence on water table depth. When β = 1, the rate increases as water table depth decreases (water table rises); when β = -1, the rate decreases as water table depth decreases.

Additional dependence on solute concentrations: Microbe-mediated redox reactions can be limited by the concentrations of electron donor (e.g., dissolved organic carbon) and / or electron acceptors. This is often the case in deep zone where organic materials are less reactive and electron acceptors such as O_2 are limited. In that case reaction rates follow the Monod form (Monod, 1949)

$$r = kA \prod_{ii=1}^{mm} \left(\frac{C_{ii}}{C_{ii} + K_{M,ii}}\right) \quad (9)$$

Here $K_{M,ii}$ is the half saturation coefficient (mol/l) of electron donor or acceptor ii and mm is the total number of electron donors and acceptors that are limiting.

In addition, when multiple electron acceptors coexist, the sequence of redox reactions occur following the biogeochemical redox ladder (Schlesinger & Bernhardt, 2020). This can be accomplished by including inhibition terms in the following form (Li, 2019; Van Cappellen & Gaillard, 1996).

$$r = kA \prod_{ii=1}^{mm} \left(\frac{C_{ii}}{C_{ii} + K_{M,ii}} \right) \prod_{j=1}^{nn} \left(\frac{K_{I,j}}{C_j + K_{I,j}} \right) \quad (10)$$

Here $K_{I,j}$ is the inhibition coefficient (mol/l) of inhibitor j and nn is the total number of inhibitors. For rates of reactions that use nitrate as electron acceptor, the inhibition term can include concentration of inhibitor O_2, as O_2 has to be almost depleted for denitrification to become dominant.

These detailed reaction rate laws are typically developed in relatively small-scale, controlled experimental systems, often well-mixed reactors, where concentrations of all participating chemicals are measured. The use of these rate laws requires concentrations of all involved species. In the natural systems, we often do not have concentration data of all participating chemicals and how they limit each other. We additionally often have limited information on spatial heterogeneities of minerals and substrate materials and which minerals are effectively reacting. Typically, we can only infer rates from measured data. As a result, we often have to simplify these rate laws and use relatively crude representation of reaction rates that involve less parameters.

2.4 Numerical scheme

The numerical scheme used is similar to those in BioRT-Flux-PIHM (Zhi et al., 2022) with some slight modifications. Sequential noniterative approach (SNIA), an operator splitting method that solves transport and reaction separately, was used in solving the equations (Steefel & MacQuarrie, 1996; Walter et al., 1994). Transport was solved using Backward Euler method, while reactions were solved iteratively using Crank-Nicholson and Newton-Raphson method with adaptive time steps. The system of linear equations derived from the discretization of ordinary differential equations (ODE)

at each step was solved using CVODE, a numerical ODE solver in SUite of Nonlinear and Differential / ALgebraic equation Solvers (SUNDIALS) (Hindmarsh et al., 2005).

2.5 Model setup and input/output

The model structure and setup of BioRT-HBV is shown in Figure 2. The input of HBV-light includes time series of precipitation, temperature, potential evapotranspiration and stream discharge (for calibration) (Seibert, 2005). HBV-light can be calibrated either manually or using automatic methods like genetic algorithm optimization (Seibert, 2000; Seibert & Vis, 2012; Vis et al., 2015). Monte Carlo simulations have also been used to pick cases that reproduce streamflow data (Sadayappan et al., 2023). Modelled water fluxes and storage from HBV are used as the hydrological input for BioRT. Model also back calculates variables that are not included in the results file of HBV, for example, amount of water percolating from upper to lower zone and form of precipitation (snowfall or rainfall), using HBV model parameters.

Depending on research needs, users can decide the complexity of the reaction network, including the type and number of reactions, and the number of solutes and sediments to be included. The information can be prescribed by users in the input files. Reaction stoichiometry, thermodynamics, and kinetics can be specified in the input files and in the geochemical database. The database follows the format of the Crunchflow model database (Steefel, 2009). The model input also includes watershed characteristics including passive water storage, porosity, depths of shallow and deep zones as well as initial concentrations of primary species that serve as the building blocks of chemical systems, mineral specific surface area and the dependence functions (soil moisture, temperature and water table depth) for reactions in both shallow and deep zones. Subsurface properties, including, for example, porosity and surface areas of reacting materials are considered as constant because the time scales considered in BioRT span from days to years.

The model output includes concentrations of different solutes and sediments in snow, surface zone, shallow zone, deep zone, and streams, as well as rates of the kinetically controlled reactions in these zones. BioRT can be run at any time scale, as long as the time intervals are consistent across input files and in both HBV-light and

BioRT models. For example, if the time series of temperature and precipitation of HBV-light inputs are at the daily scale, the input of precipitation chemistry for BioRT should also be at the daily scale. The output of BioRT will also be correspondingly at the daily scale. If instead the precipitation and all other inputs are at minute or hourly scales for events, the output will be at the same time scale.

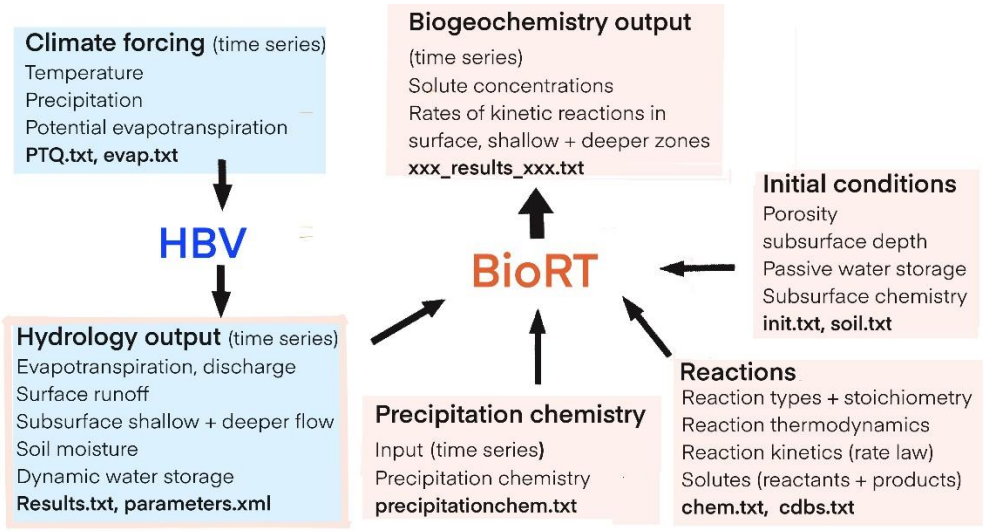

Figure 2. *The model structure of BioRT-HBV. HBV-light and BioRT need to be run separately. HBV requires climate forcing as input, and outputs time series of water variables that quantify water balance and surface and subsurface flow. The model output of HBV is used as input for BioRT, along with other input files that describe the chemical forcing, initial conditions, and reactions. BioRT output includes time series of solute concentrations in different zones and in stream and reaction rates in different zones.*

3. EXAMPLE MODEL APPLICATIONS

BioRT has been used to understand reactive transport processes in multiple watersheds, including the catchment W-9 in Sleepers River in Vermont (Stewart et al., 2023, in review), and Coal Creek in Colorado (Kerins et al., 2023, in review). Here we showcase the application of BioRT in W-9 in Vermont, US. We first describe W-9 catchment and its hydrology to provide context, followed by the simulation of carbon and nitrogen processes. Carbon processes modelled include soil respiration (lumped heterotrophic and autotrophic respiration) that produces Dissolved Organic Carbon (DOC) and Dissolved Inorganic Carbon (DIC), adsorption of DOC to soils, and carbonate weathering. Nitrogen (N) processes include N leaching, plant N uptake, and denitrification. The carbon processes were calibrated using stream chemistry, whereas

the nitrogen processes are presented as an uncalibrated example. These reaction examples are not meant to be comprehensive but serve the purpose of illustrating what can be done using BioRT.

3.1 Study site

W-9 is a small, forested headwater catchment (0.405 km^2) in the Sleepers River Research Watershed in northeastern Vermont, USA. It has a humid continental climate with mean annual precipitation of 1320 mm and mean annual temperature of 4-6°C (Armfield et al., 2019; Sebestyen et al., 2009). Approximately 20-30% of annual precipitation falls as snow; 40% of precipitation is partitioned to evapotranspiration, while the remaining 60% is partitioned to stream runoff (Shanley, 2000). Soils on hillslopes are well-drained inceptisols and spodosols while riparian soils are poorly drained histosols. The catchment is underlain by quartz-mica schist and carbonate-containing calcareous granulite bedrock (Shanley, 2000; Shanley et al., 2004). Weathering of carbonate minerals (mostly calcite) produces base cations like calcium (Ca) and carbonate species, resulting in well-buffered subsurface and stream water (Adler et al., 2021; Shanley, 2000).

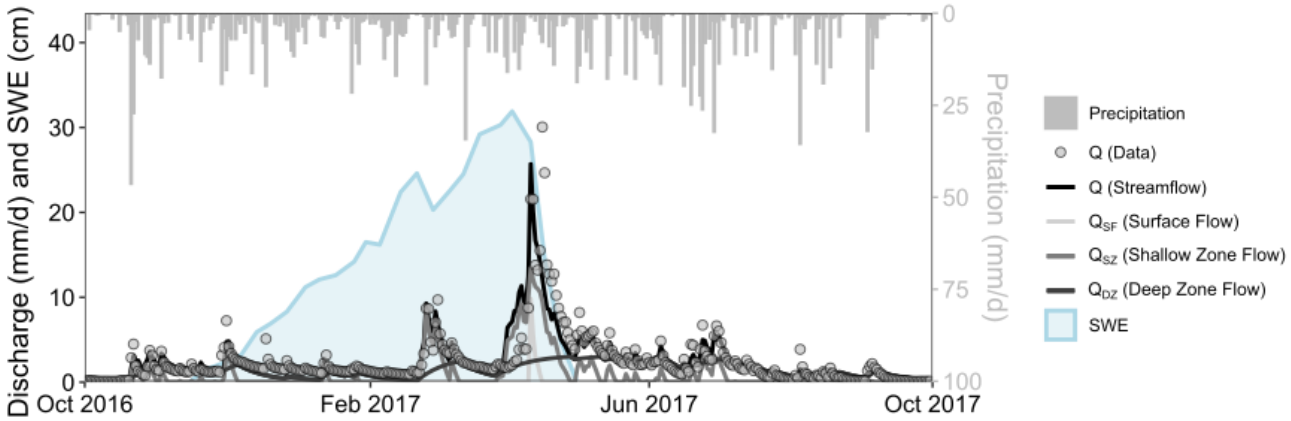

Figure 3: *Time series of observed precipitation, discharge, snow water equivalent (SWE) and HBV model output (lines) that reproduces stream discharge data (dots) at W-9 for water year 2017.*

W-9 is a seasonally snow-dominated catchment. Discharge often peaks in March or April following spring snowmelt (Figure 3). Model output from HBV suggests that annual discharge is dominated by deep flow Q_{DZ} (~64%), followed by shallow flow Q_{SZ}

(~35%) and minimal contributions from Q_{SF} (~1%). At the daily scale, shallow flow Q_{SZ} often dominates under wet conditions (e.g., spring snowmelt) and Q_{DZ} dominates under dry conditions (e.g., summer). This partitioning of discharge is consistent with previous studies that highlight a strong groundwater signature in baseflow stream chemistry and new water contributions through surficial soils and shallow flow paths following events like snowmelt and storms (Kendall et al., 1999; Sebestyen et al., 2008; Shanley et al., 2002; Shanley et al., 2015).

3.2 Carbon processes

3.2.1 Reaction network

To understand the dynamics of dissolved carbon in the stream, we simulate both carbonate weathering (carbonate lithology at W-9) and soil respiration, including heterotrophic respiration (carbon decomposition) by microbes and autotrophic respiration by plant roots, among other reactions (Table 1). Three reactions were included to capture DOC dynamics: shallow zone soil respiration ($Resp_{SZ}$), deep zone respiration ($Resp_{DZ}$), and equilibrium-controlled sorption in shallow zone ($Sorption_{SZ}$). $Resp_{SZ}$ represents the net DOC and DIC production from microbial processing of soil organic carbon (OC_{SZ}) and root respiration and exudates ($Roots_{DOC\&DIC}$). $Resp_{DZ}$ represents DIC produced in the DZ where, in addition to translocated DOC from the shallow zone, petrogenic carbon (Dean, 2019; Soulet et al., 2018) and deep root exudates (Tune et al., 2020) can also act as sources of DIC. We use the temperature dependence function (f(T) in equation (6)) to account for the generally higher respiration rates in the summer, and the soil moisture function ($f(S_w)$) to account for rate dependence on water content. These reactions are considered as occurring only in the shallow and deep zones, as their occurrence at the ground surface tends to be minimal due to fast runoff and short contact time with surface materials.

The carbonate weathering reactions, $Carbonate_{SZ}$ and $Carbonate_{DZ}$, represent the dissolution of carbonate-containing minerals to produce calcium ions (Ca^{2+}) and DIC (via CO_3^{2-}) following a TST rate law. $Carbonate_{DZ}$ follows the same reaction as $Carbonate_{SZ}$, though reaction rates and stoichiometry differ due to differences in the origin and composition of carbonate in the two zones. The shallow zone carbonate is

usually pedogenic carbonate generated by carbonate precipitation in soil under dry conditions (Macpherson & Sullivan, 2019; Zamanian et al., 2016), whereas deep zone carbonate is typically partially weathered or unweathered carbonate bedrock.

DIC is the sum of all dissolved inorganic carbon species (CO_2(aq), HCO_3^- and CO_3^{2-}). The model simulates carbonate speciation reactions between these three species, depending on pH. High concentration of CO_2(aq) leads to the formation of CO2 gas in soil. The extent of this CO_2 gas-aqueous exchange is determined by CO_2 solubility prescribed by Henry's Law. In BioRT, we represent CO_2(*g) as an immobile pseudo-gas phase that can dissolve to become CO_2(aq). DIC production and CO_2 gas-aqueous exchange are coupled processes so they are always simulated together. The full reaction network and calibrated parameters are summarized in Table 1.

Table 1. Reaction network and parameters for BioRT-HBV model calibrated for respiration and weathering in W-9 catchment of Sleepers River.

Reactions	Rate law	$\log_{10}$ Keq	$\log_{10}k$ (mol/ m^2/s)	SSA (m^2/g)	$f(T)$ Q_{10}	$f(S_w)$ n, $S_{w,c}$	$f(Z_w)$ α × β
Shallow Zone Reactions							
(1) Respiration ($Resp_{SZ}$): $OC(s) + Roots_{DOC\ \&\ DIC} \rightarrow 0.6DOC + 0.55DIC$	$r1 = kAf(Z_w)f(T)f(S_w)$	NA	-10.2	0.10	2.30	0.8, 0.7	0
(2) Carbonate$_{SZ}$: $Carbonate_{SZ}(s) \rightarrow 1.1Ca^{2+} + 0.5DIC$	$r2 = kA\left(1 - \frac{IAP}{K_{eq}}\right)$	-7.60	-9.19	1.00	1.00	1.0, 1.0	0
(3) Sorption ($Sorption_{SZ}$): $\equiv X + DOC \leftrightarrow \equiv XDOC$	$Equilibrium\ reaction$	-1.00	NA	1.0	NA	NA	NA
(4) CO_2 Gas – Aqueous Exchange: $CO_2(*g) \leftrightarrow CO_2(aq)$	$r4 = kA\left(1 - \frac{IAP}{K_{eq}}\right)$	-3.20	-13.10	0.01	3.0	0.7, 0	0
Deep Zone Reactions							
(5) $Resp_{DZ}$: $OC_{DZ}(s) + DOC \rightarrow 0.7DIC$	$r5 = kAf(Z_w)f(T)f(S_w)$	NA	-9.2	0.07	1.00	1.2, 0.6	0

(6) Carbonate$_{DZ}$: $Carbonate_{DZ}(s) \rightarrow 0.9Ca^{2+} + 0.7DIC$	$r6 = kA\left(1 - \frac{IAP}{K_{eq}}\right)$	-7.30	-9.19	7E-4	3.00	0.9, 1.0	0
(7) CO_2 Gas – Aqueous Exchange: $CO_2(*g) \leftrightarrow CO_2(aq)$	$r7 = kA\left(1 - \frac{IAP}{K_{eq}}\right)$	-3.20	-13.10	7E-3	1.5	0.7, 0	0
Equilibrium Reactions in both Shallow and Deep Zones							
Carbon Speciation Reactions							
(8) $CO_2(aq) + H_2O \leftrightarrow HCO_3^- + H^+$	$Equilibrium\ reaction$	-6.35	NA	NA	NA	NA	NA
(9) $HCO_3^- \leftrightarrow CO_3^{2-} + H^+$	$Equilibrium\ reaction$	-10.33	NA	NA	NA	NA	NA

*The gas-aqueous exchange represents the exchange reactions between soil CO_2 (CO_2(*g) and dissolved CO_2 ($CO_{2(aq)}$). NA means the parameter is not applicable for the particular reaction network.

3.2.2 Reactive transport equations

In this particular example, the primary species are DOC, CO_2(aq), Ca^{2+}, H^+, and $\equiv X$; the secondary species are CO_3^{2-}, HCO_3^-, OH^- and $\equiv XDOC$. Dissolved inorganic carbon (DIC) is the summation of CO_2(aq), HCO_3^- and CO_3^{2-}. We solve equations (1) – (3) for the concentrations of all primary species. Other solutes, including HCO_3^- and CO_3^{2-}, are expressed via equilibrium relationships with CO_2(aq) after time stepping for the primary species. The overall reaction rate R (R_{SF}, R_{SZ}, R_{DZ} in equations (1) – (3)) for each primary species could be the summation of multiple rates from different reactions. For example, Ca^{2+} is only involved in carbonate weathering, such that the R_{SZ} and R_{DZ} terms in its equation (2) and (3) only include rate expressions for reactions (2) and (6) and the corresponding reaction stoichiometric coefficients in Table 1, respectively. In other words, $R_{SZ} = \alpha_{2,Ca} r_2 = 1.1\ r_2$, and $R_{DZ} = \alpha_{6,Ca} r_2 = 0.9\ r_6$. For CO_2(aq), $R_{SZ,\ CO2(aq)} = \alpha_1 r_1 + \alpha_2 r_2 + \alpha_4 r_4$, as there are three kinetic reactions involved in contributing to different forms of DIC. The α values in front of r refer to the reaction stichometry coefficients corresponding to the species specified in the "Reactions" column in Table 1. Similarly, $R_{DZ,\ CO2(aq)} = \alpha_5 r_5 + \alpha_6 r_6 + \alpha_7 r_7$.

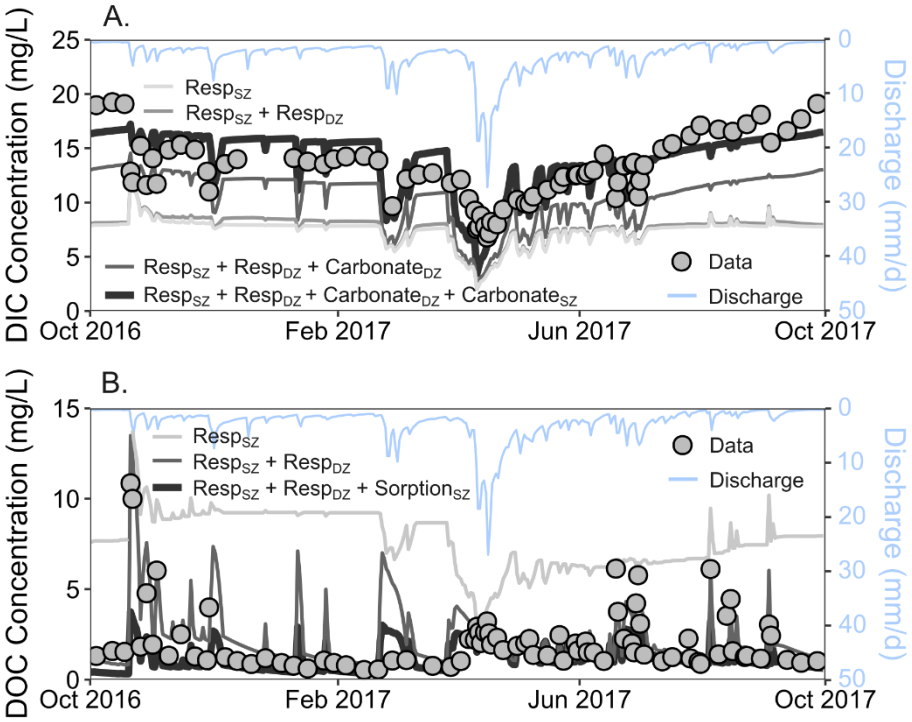

Figure 4: *BioRT-HBV model output of stream concentrations (mg/l) for A. Dissolved Inorganic Carbon (DIC) and B. Dissolved Organic Carbon (DOC). The different lines are different model outputs when including different reactions ($Resp_{SZ}$, $Resp_{DZ}$, $Sorption_{SZ}$, $Carbonate_{SZ}$, and $Carbonate_{DZ}$); the lines are compared to data (dots) to illustrate how much they capture the dynamics in data. Stream DIC concentrations are only reproduced by the model when all reactions are included, indicating that both carbonate and respiration sources are important. DOC is primarily produced via soil respiration ($Resp_{SZ}$) and consumed via deep respiration ($Resp_{DZ}$). The model without deep respiration overestimates DOC and produces opposite trend of DOC from data (low DOC at high discharge), underscoring the importance of deep respiration. The sorption reaction ($Sorption_{SZ}$) acts as a buffer and reduces the overall stream concentrations of DOC, particularly peak concentrations.*

3.2.3 Interrogating model with data to understand influential reactions

Stream chemistry reflect the influence of multiple reactions such that it is often challenging to differentiate the role of individual reactions. Here we illustrate that the model can be used to distinguish the role of different reactions in determining stream solute dynamics (Figure 4A). For example, when $Resp_{SZ}$ is the only reaction included in the simulation, modeled DOC concentrations are high throughout the year, rather than only at high flow conditions as indicated by observations. Adding deep respiration $Resp_{DZ}$ reduces the low flow concentrations of DOC as the deep zone reaction consumes DOC from the shallow zone, thereby reducing DOC concentrations in the DZ and bringing the modeled DOC closer to data. This indicates that deep zone DOC

consumption is an important process. Stream DOC is also influenced by sorption of DOC onto soils in SZ ($Sorption_{SZ}$). Sorption is more likely to occur in SZ due to the typically higher clay content. Sorption stores some of produced DOC on soil surface such that not all DOC is flushed to the stream at high discharge. In other words, some DOC is retained and stored on soils in the SZ, which is consistent with field observations (Neff & Asner, 2001) and observations in other places (Wen et al., 2020). When only including respiration in the model, modelled DIC concentrations in the stream are lower than measured DIC, regardless of $Resp_{SZ}$ model parameters, indicating the presence of an additional DIC source (Figure 4 B). When including carbonate weathering, stream DIC concentrations from the model agree better with data, suggesting that both biogenic and geogenic sources contribute to stream DIC.

3.2.4 Dissolved carbon concentrations in the subsurface and stream

The calibrated model can be used to understand carbon processes on land and in streams (Figure 5). Simulation outputs show that concentrations of DIC and Calcium (Ca) are higher in the DZ than the SZ. Correspondingly, stream DIC and Ca concentrations at low flow conditions dominated by groundwater are generally high. During high discharge, stream DIC and Ca are diluted by the large input of shallow soil water with low Ca and DIC, as demonstrated in the negative, or dilution, relationships between concentration and discharge for both solutes. Concentrations of DOC are lower in the DZ than in the SZ, such that stream concentrations are low when DZ water dominates at low discharge and increase with discharge as Q_{SZ} increasingly contributes to streamflow. This leads to a positive, or flushing, relationships between concentration and discharge. Stream DIC and Ca concentrations are relatively stable compared to DOC but exhibit a more pronounced seasonal trend with lowest concentrations in early spring (~April) and highest concentrations in late summer (~September).

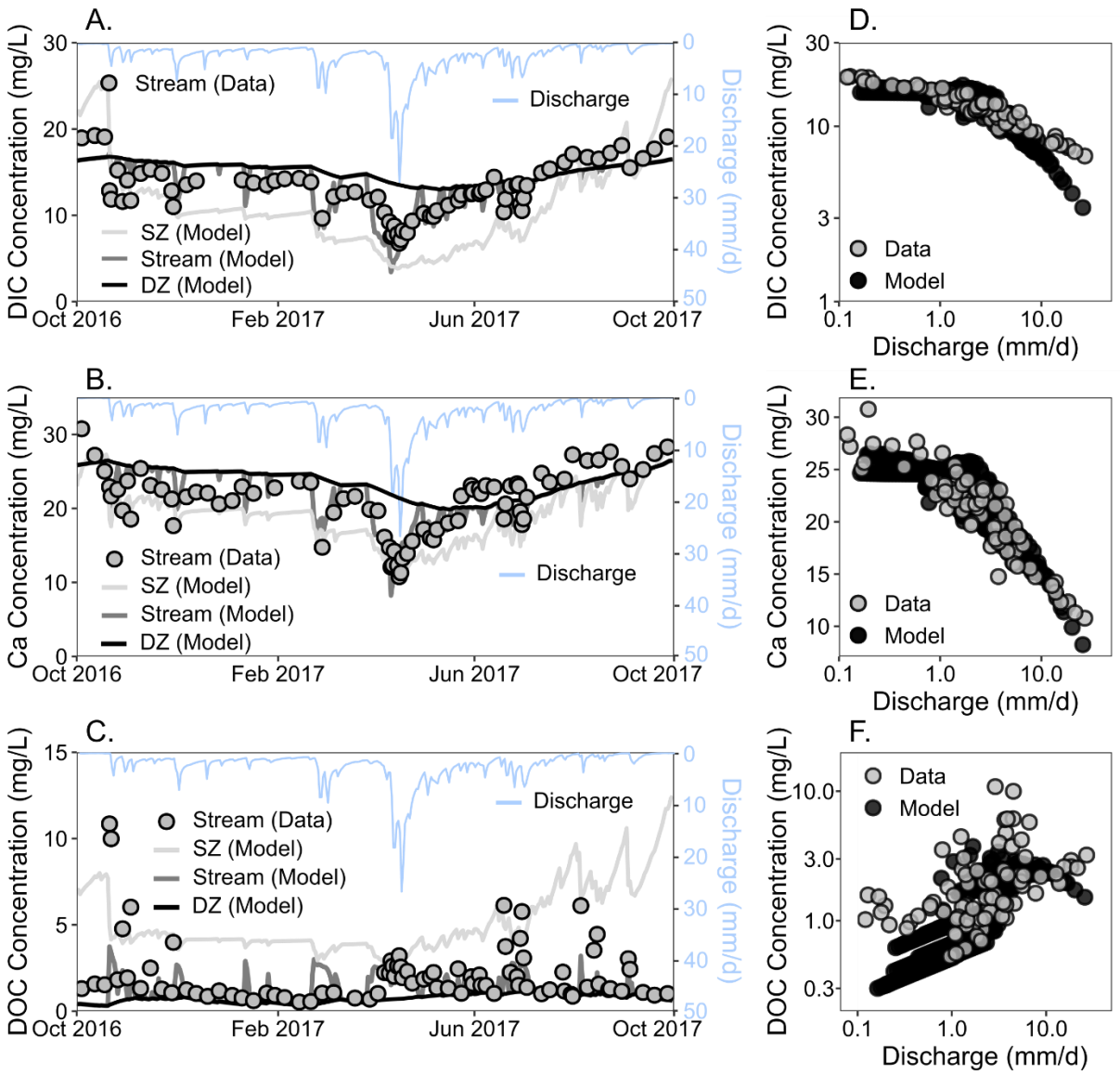

523

524 ***Figure 5:*** *Time series of data and modeled concentrations (mg/l) in stream, shallow zone (SZ),*
525 *and deep zone (DZ) for A. Dissolved Inorganic Carbon (DIC), B. Calcium (Ca), C. Dissolved*
526 *Organic Carbon (DOC). Concentration-discharge plots for stream chemistry data and model*
527 *output for D. DIC, E. Ca, F. DOC.*

528 **3.2.5 Carbon reaction rates and export dynamics**

529 In addition to understanding the processes that regulate stream chemistry, the
530 calibrated model can also be used to understand the temporal trends and dependence
531 of reaction rates and export patterns (Figure 6). The model simulation shows that
532 carbonate weathering rates in the SZ ($Carbonate_{SZ}$) vary significantly (Figure 6).
533 $Carbonate_{SZ}$ has baseline rate of 0, indicating when the carbonate mineral is at

equilibrium with water. The reaction can increase to positive values indicating dissolution, or decrease to negative values indicating calcite precipitation (mostly in summer months at low discharge). The soil respiration rate $Resp_{SZ}$ shows a strong seasonal trend, with highest rates in warm, summer months and lowest rates in cool, winter months. In the deep zone, rates are slower overall; $Carbonate_{DZ}$ exhibits less flashy dynamics than $Carbonate_{SZ}$ and a similar seasonal trend to $Resp_{SZ}$ with higher rates in summer months and lower rates in winter months. Deep respiration ($Resp_{DZ}$) rates, however, show more drastic seasonal behavior with highest rates in spring and lowest rates in autumn and late winter. This is because high flow in spring leads to high recharge and more transport of DOC to the DZ, facilitating deep respiration. Export rates from the SZ are flashy with high peak during high discharge, while export rates from the DZ are more stable due to steady contributions of groundwater flow (Q_{DZ}) to the stream. Ca and DIC are exported from both the SZ and DZ, though export from the DZ is more persistent. DOC is primarily exported from the SZ; DOC export from the DZ is negligible.

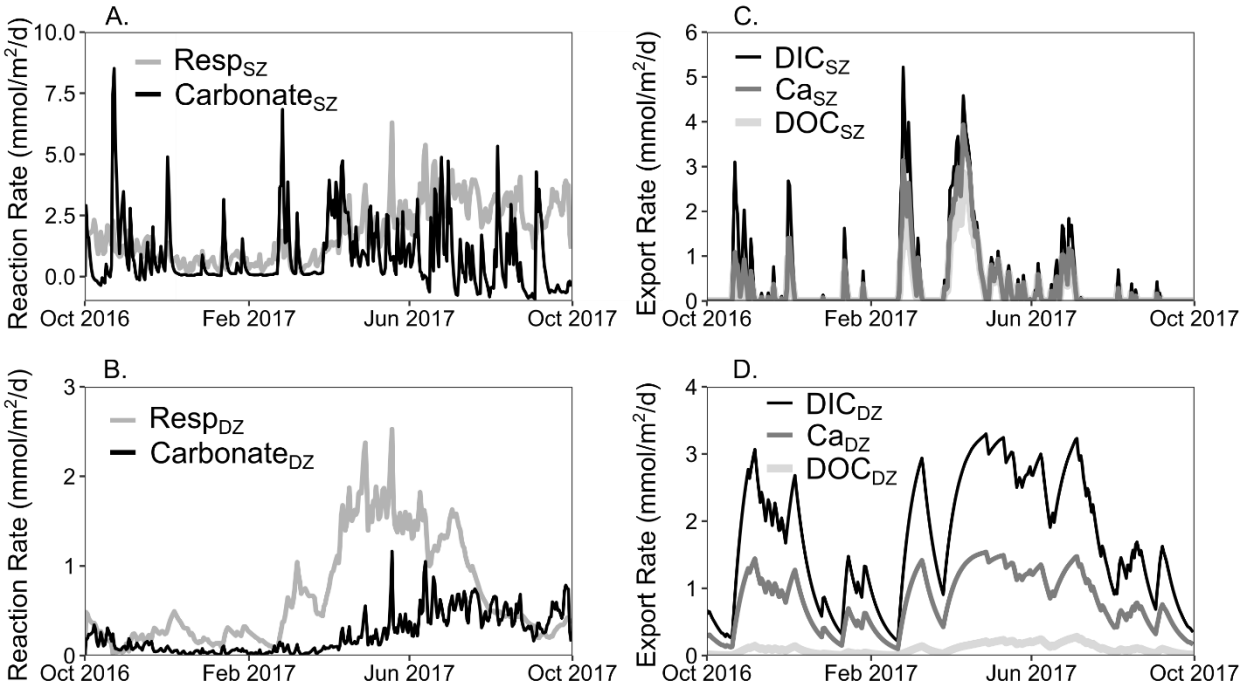

Figure 6: *Time series of modeled reaction rates (mmol/m²/d) in A. shallow zone (SZ) and B. deep zone (DZ); Time series of export rates (mmol/m²/d) for Ca, DIC, and DOC from the C. SZ and D. DZ. Reactions include $Resp_{SZ}$, $Carbonate_{SZ}$, $Resp_{DZ}$, and $Carbonate_{DZ}$.*

3.3 Nitrogen processes

3.3.1 Reaction network

BioRT can also be used to explore the role of different reactions in determining concentrations, rates, and stream chemistry dynamics in numerical experiments. Here we demonstrate such capability using processes related to nitrate. Nitrate is an essential component in biogeochemical cycles and can contribute to greenhouse gas emissions. It is also a ubiquitous contaminant that has caused widespread eutrophication and hypoxia, leading to widespread interest in understanding its dynamics (Z. W. Ma et al., 2023; Sadayappan et al., 2022; Van Meter et al., 2018). For simplicity, we include three biogeochemical reactions that produce and consume nitrate (NO_3^-): soil nitrogen (N) leaching, plant uptake of NO_3^-, and denitrification (Table 2). Soil N leaching is a lumped reaction that represents the net rates of soil organic matter (SOM) decomposition, nitrification, and rock weathering processes that generate NO_3^-. Plant uptake is represented by a simple approach that accounts for NO_3^- removal from water by plant assimilation. The denitrification reaction is represented with NO_3^- being fully reduced to N_2O although NO_3^- can also be reduced to N_2 and a suite of other N-containing solutes. These reactions all follow the simplified rate law $r = kAf(T)f(S_w)f(Z_w)$ (Equation 5), without explicitly considering dependence on other solutes.

Table 2. Reaction network and parameters for nitrate processes in BioRT-HBV model

Reactions	Rate law	$\log_{10}k$ (mol/ m^2/s)	SSA (m^2/g)	$f(T)$ Q_{10}	$f(S_w)$ n, $S_{w,c}$	$f(Z_w)$ α × β
Shallow Zone Reactions						
Nitrogen Leaching ($NLeaching_{SZ}$): $soilN \rightarrow NO_3^-$	$r = kAf(Z_w)f(T)f(S_w)$	-15.0	5.5	2.0	1, 1.7	0
Plant Uptake ($PlantUptake_{SZ}$): $NO_3^- \rightarrow PlantN$	$r = kAf(Z_w)f(T)f(S_w)$	-13.4	3.0	1.5	1, 1.25	0
Denitrification ($Denitrification_{SZ}$): $NO_3^- \rightarrow N_2O$	$r = kAf(Z_w)f(T)f(S_w)$	-12.8	1E-6	1.0	1, 0	0

Deep Zone Reactions						
NLeaching$_{DZ}$: $soilN \rightarrow NO_3^-$	$r = kAf(Z_w)f(T)f(S_w)$	-15.0	1E-4	1.0	1, 0	0
PlantUptake$_{DZ}$: $NO_3^- \rightarrow PlantN$	$r = kAf(Z_w)f(T)f(S_w)$	-13.4	1E-4	2.5	1, 0	0
Denitrification$_{DZ}$: $NO_3^- \rightarrow N_2O$	$r = kAf(Z_w)f(T)f(S_w)$	-12.8	3E-4	1.5	1, 0	0

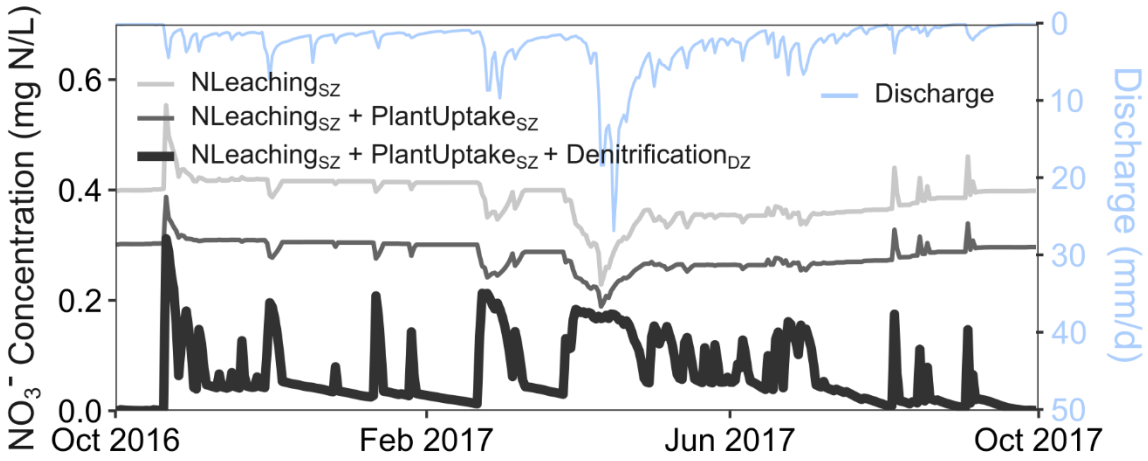

Figure 7: *BioRT-HBV model output of Nitrate (NO_3^-) concentrations (mg/l) with different reaction combinations. NO_3^- is produced by NLeaching in the shallow zone (SZ), but typical stream NO_3^- concentrations and dynamics are only reproduced when both PlantUptake$_{SZ}$ and Denitrification$_{DZ}$ reactions are included to consume NO_3^- in both the SZ and deep zone (DZ). Note that the inclusion of Denitrification$_{DZ}$ (darkest gray) led to a pattern opposite from those excluding this reaction (lighter grays).*

The example in Figure 7 illustrates the role of different types of reactions in determining stream nitrate dynamics. With only the Nleaching reaction in the SZ (NLeaching$_{SZ}$), concentrations are generally higher than other cases and show a dilution pattern (higher concentrations at low discharge conditions). Adding the plant uptake reaction reduces stream NO_3^- concentrations, but the temporal dynamics of stream NO_3^- remains similar to the case with only NLeaching$_{SZ}$. The dynamics change significantly when the denitrification reaction in the DZ (Denitrification$_{DZ}$) is included, resulting in lower concentrations during low flow but higher concentrations during high flow.

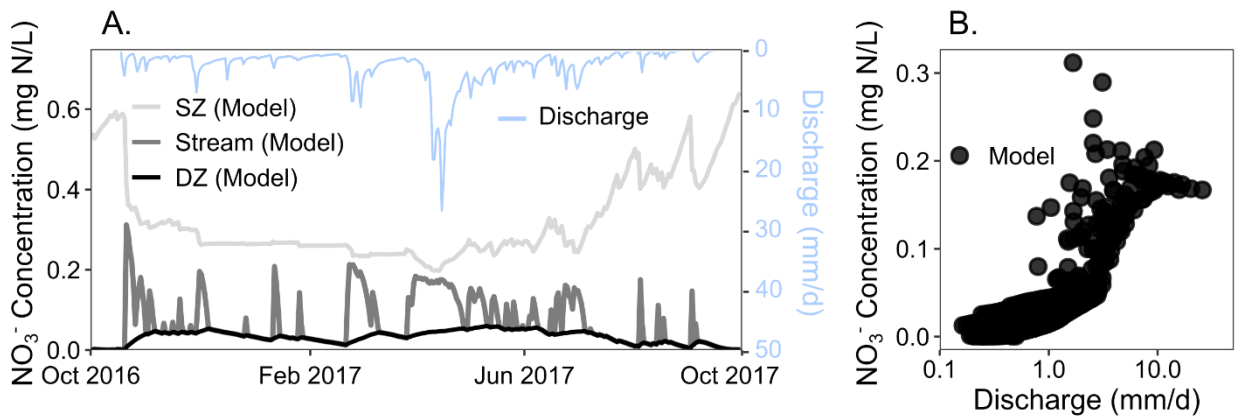

Figure 8: *A. Time series of modelled nitrate (NO_3^-) concentrations (mg/l) in stream, shallow zone (SZ), and deep zone (DZ). B. Corresponding concentration-discharge plot for modeled stream NO_3^-.*

3.3.2 Nitrate concentration dynamics, reaction rates and export dynamics

The model output in the case with all three reactions ($NLeaching_{SZ}$, $PlantUptake_{SZ}$, and $Denitrification_{DZ}$ for NO_3^-) show high nitrate concentrations in the SZ where the N leaching rate exceeds the plant N uptake rate, and low nitrate concentrations in the DZ due to denitrification (Figure 8A and 9A). As a result, high stream nitrate concentrations occur when Q_{SZ} contributes to the stream. This leads to a flushing concentration-discharge relationship (Figure 8 B) that echoes the typical flushing pattern seen in observed data (Porter et al., 2022; Stewart et al., 2022). This highlights the need for denitrification processes in subsurface to capture NO_3^- dynamics.

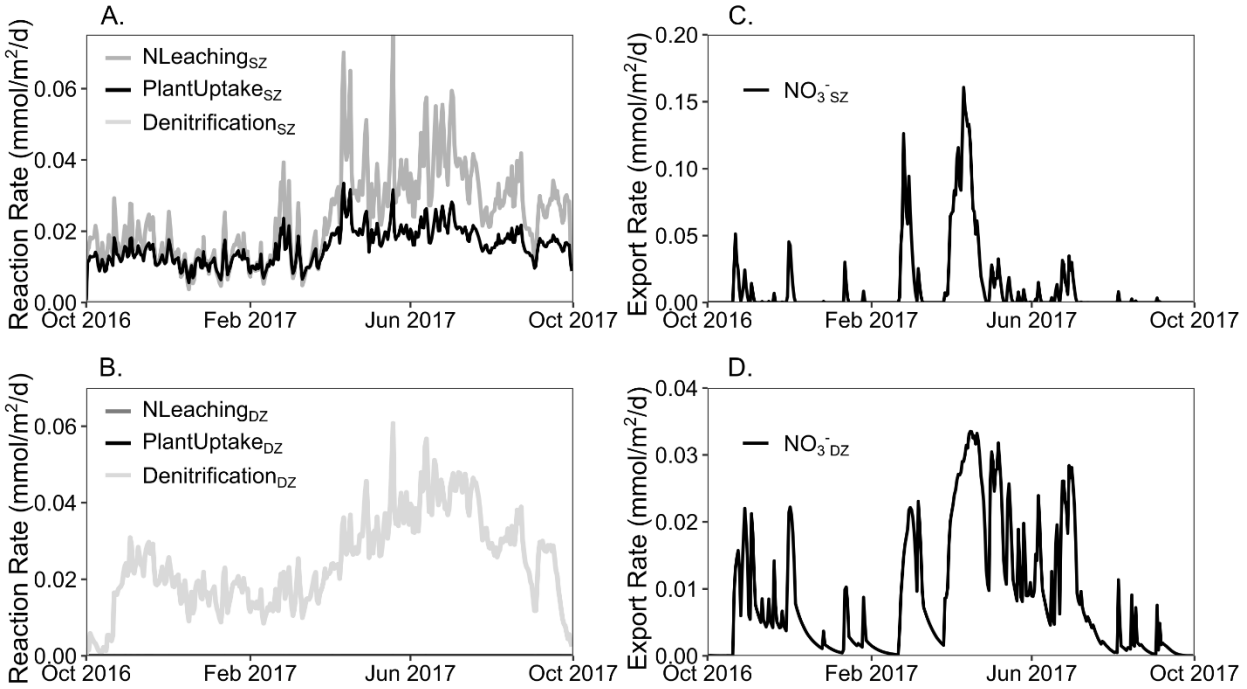

Figure 9: *Time series of overall reaction rates (mmol/m^2/d) for A. shallow zone (SZ) and B. deep zone (DZ) for NLeaching$_{SZ}$ (nitrate leaching), PlantUptake$_{SZ}$ (plant assimilation of nitrate), and Denitrification$_{DZ}$. Rates of Denitrification$_{SZ}$, NLeaching$_{DZ}$, and PlantUptake$_{DZ}$, are effectively zero. Time series of overall export rates (mmol/m^2/d) for Nitrate (NO_3^-) from the C. SZ and D. DZ.*

Nitrate leaching and plant uptake mostly occur in the SZ, whereas denitrification mostly occurs in the DZ (Figure 9). NLeaching$_{SZ}$ rates are generally lower in autumn and winter and higher in spring and summer, peaking in April and May (Figure 9A). PlantUptake$_{SZ}$ rates follow a similar pattern to NLeaching$_{SZ}$ but exhibit a smaller increase in spring and summer months. Denitrification$_{DZ}$ rates show similar seasonal dynamics to NLeaching$_{SZ}$ and PlantUptake$_{SZ}$ with lower rates in autumn and winter and higher rates in spring and summer. Hydrology and the temporal changes in flow paths determine nitrate export dynamics (Figure 9C and 9D) with high and low export rates occurring during high, Q_{SZ} dominated, and low, Q_{DZ} dominated, flow times respectively. Nitrate export occurs mainly from SZ, while DZ acts as a smaller but steadier source of nitrate to the stream. These insights align with other studies that explore the reaction and transport pathways of nitrate (Husic et al., 2019).

4. DISCUSSION

We show that BioRT-HBV, as a watershed-scale reactive transport model, can simulate both surface and subsurface flow paths, and biogeochemical reactions that are influenced by hydroclimatic conditions and land-surface interactions. BioRT-HBV builds upon the widely used HBV hydrology model, inheriting its structural framework. Additionally, it maintains the traditional capability of reactive transport models (RTMs) to flexibly and adaptively (to needs of the users) represent a variety of user-defined biogeochemical reactions.

In the realm of modeling, there has been an ongoing debate about the advantages and disadvantages of simple versus complex models (Wen et al., 2021). Complex models, such as spatially distributed, nonlinear, multi-component RTMs, can represent and explore the effects of spatial heterogeneities in watershed properties (e.g., soil depth and types, lithology, vegetation, biomass, and mineralogy) on catchment-scale dynamics including streamflow generation and stream concentration dynamics and solute export patterns (Fatichi et al., 2016; Li et al., 2021). However, these models are computationally demanding and present difficulties for ensemble-based analysis. These models also require extensive data and have large number of parameters that lead to issues related to equifinality and uncertainty (Beven, 2006; Beven & Freer, 2001; Kirchner et al., 1996).

Parsimonious models can overcome some of these outstanding challenges. It is in this context of balancing the cost and gain that we developed the BioRT-HBV model (Li et al., 2021). This spatially implicit bucket model requires minimal data and is computationally inexpensive. The model does not resolve spatial details and cannot explicitly explore features such as “hot spots” of biogeochemical reactions (Wen et al., 2020). The model represents the “average” dynamics of water flow and reactions on land and in rivers at the watershed scale that are eventually reflected in commonly measured stream chemistry data. This lumped approach can accommodate basins with low data availability, and is more accessible to users from diverse backgrounds, such that process-based models are not limited to a small group of users with extensive modeling and computational experience. Ultimately, the choice of the model complexity level depends on research questions that the model is set to answer and the available data. At the end, we all need to balance cost and gain when deciding to use a simple or

complex model, striving to be “simple but not simplistic” (Beven & Lane, 2019; Höge et al., 2018; Li et al., 2021).

An additionally important, often overlooked aspect is the accessibility of models, especially in terms of the user's experience and knowledge. Models that are straightforward and easy to understand are more user-friendly for those without in-depth computational training. This makes them valuable educational tools, as demonstrated by the success of HBV-light (Seibert & Bergström, 2022). Easily accessible models can also promote their widespread use across different fields, boosting interdisciplinary research. Furthermore, these models can help foster a more varied and inclusive user community, supporting diversity, equity, and inclusion (DEI).

5. CONCLUSION

Watershed-scale Reactive Transport Models (RTMs) are vital for understanding and predicting the complex interactions of ecohydrological and biogeochemical processes that influence water chemistry and fluxes on land and in rivers. While traditional RTMs have mainly concentrated on subsurface processes, recent advancements have expanded RTMs to encompass interactions between surface and subsurface environments at the watershed scale. These advanced RTMs are notable for their intricate spatial detail and computational intensity, though their complexity also presents challenges. There is a growing need for simple, user-friendly models that can serve the broader ecohydrological and biogeochemical research community, including those without deep computational experience.

To address this, we introduce BioRT-HBV 1.0 (BioRT), a new, simple watershed-scale model that integrates ecohydrological and biogeochemical processes. BioRT builds upon the extensively-used HBV model and uses its conceptual framework and hydrology outputs. BioRT simulates various processes such as solute transport and biogeochemical reactions governed by thermodynamics and kinetics, including chemical weathering, soil respiration, and nutrient transformations. This paper outlines its model structure and governing equations and demonstrates example applications through case studies simulating carbon and nitrogen processes in a headwater catchment. BioRT-HBV model has a simple structure and minimal data requirement, yet can

simulate a variety of biogeochemical processes that occur in the invisible subsurface. We put forward BioRT as an easily accessible tool for researchers irrespective of their computational expertise.

DATA AVAILABILITY

BioRT-HBV 1.0 model is open source and available for download at https://github.com/Li-Reactive-Water-Group/BioRT-HBV/tree/V-1.0. The input files used for simulating carbon and nitrogen processes are also available there.

ACKNOWLEDGEMENT

The work is supported by US National Science Foundation (EAR 2012123, EAR-2012669, EAR-2121621, EAR-2034214, EAR-1904527) and US Department of Energy Earth and Environmental system program (DE-SC0020146).

REFERENCES

Aagaard, P., & Helgeson, H. C. (1982). Thermodynamic and Kinetic Constraints on Reaction-Rates among Minerals and Aqueous-Solutions .1. Theoretical Considerations. *American Journal of Science, 282*(3), 237-285. <Go to ISI>://WOS:A1982NH17800002

Adler, T., Underwood, K. L., Rizzo, D. M., Harpold, A., Sterle, G., Li, L., et al. (2021). Drivers of Dissolved Organic Carbon Mobilization From Forested Headwater Catchments: A Multi Scaled Approach. *Frontiers in Water, 3*.

Anderson, S. P., Dietrich, W. E., Torres, R., Montgomery, D. R., & Loague, K. (1997). Concentration-discharge relationships in runoff from a steep, unchanneled catchment. *Water Resources Research, 33*(1), 211-225.

Andersson, L., Rosberg, J., Pers, B. C., Olsson, J., & Arheimer, B. (2005). Estimating catchment nutrient flow with the HBV-NP model: Sensitivity to input data. *Ambio, 34*(7), 521-532. <Go to ISI>://WOS:000233522100007

Arheimer, B., & Brandt, M. (1998). Modelling nitrogen transport and retention in the catchments of southern Sweden. *Ambio, 27*(6), 471-480. <Go to ISI>://WOS:000077140400010

Arheimer, B., Dahne, J., Donnelly, C., Lindström, G., & Stromqvist, J. (2012). Water and nutrient simulations using the HYPE model for Sweden vs. the Baltic Sea basin - influence of input-data quality and scale. *Hydrology Research, 43*(4), 315-329. <Go to ISI>://WOS:000306235400002

Arheimer, B., Lowgren, M., Pers, B. C., & Rosberg, J. (2005). Integrated catchment modeling for nutrient reduction: Scenarios showing impacts, potential, and cost of measures. *Ambio, 34*(7), 513-520. <Go to ISI>://WOS:000233522100006

Arheimer, B., & Wittgren, H. B. (1994). Modeling the Effects of Wetlands on Regional Nitrogen Transport. *Ambio, 23*(6), 378-386. <Go to ISI>://WOS:A1994PN58600010

Armfield, J. R., Perdrial, J. N., Gagnon, A., Ehrenkranz, J., Perdrial, N., Cincotta, M., et al. (2019). Does Stream Water Composition at Sleepers River in Vermont Reflect Dynamic Changes in Soils During Recovery From Acidification? *Frontiers in Earth Science, 6*.

718 Bai, J. H., Zhang, G. L., Zhao, Q. Q., Lu, Q. Q., Jia, J., Cui, B. S., & Liu, X. H. (2016). Depth-distribution
719 patterns and control of soil organic carbon in coastal salt marshes with different plant covers.
720 *Scientific Reports, 6*. <Go to ISI>://WOS:000384763000001
721 Bao, C., Li, L., Shi, Y., & Duffy, C. (2017). Understanding watershed hydrogeochemistry: 1. Development
722 of RT-Flux-PIHM. *Water Resources Research, 53*(3), 2328-2345.
723 http://dx.doi.org/10.1002/2016WR018934

724 http://onlinelibrary.wiley.com/store/10.1002/2016WR018934/asset/wrcr22511.pdf?v=1&t=j34tmu4n&
725 s=bdf81c580440d11b93f8793bbc653f73be04fc2b
726 Bastrup-Birk, A., & Gundersen, P. (2004). Water quality improvements from afforestation in an
727 agricultural catchment in Denmark illustrated with the INCA model. *Hydrology and Earth System*
728 *Sciences, 8*(4), 764-777. <Go to ISI>://WOS:000226829900016
729 Bergström, S. (1992). The HBV model-its structure and applications.
730 Bergström, S., Brandt, M., & Gustafson, A. (1987). Simulation of runoff and nitrogen leaching from two
731 fields in southern Sweden. *Hydrological sciences journal, 32*(2), 191-205.
732 Bergström, S., Carlsson, B., Sandberg, G., & Maxe, L. (1985). Integrated Modeling of Runoff, Alkalinity,
733 and Ph on a Daily Basis. *Nordic Hydrology, 16*(2), 89-104. <Go to ISI>://WOS:A1985ALW0700004
734 Bergström, S., & Forsman, A. (1973). Development of a conceptual deterministic rainfall-runoff mode.
735 *Nord. Hydrol, 4*, 240-253.
736 Bergström, S., & Lindström, G. (2015). Interpretation of runoff processes in hydrological modelling
737 experience from the HBV approach. *Hydrological Processes, 29*(16), 3535-3545. <Go to
738 ISI>://WOS:000358446700008
739 Beven, K. (2006). A manifesto for the equifinality thesis. *Journal of Hydrology, 320*(1-2), 18-36.
740 Beven, K., & Freer, J. (2001). Equifinality, data assimilation, and uncertainty estimation in mechanistic
741 modelling of complex environmental systems using the GLUE methodology. *Journal of*
742 *Hydrology, 249*(1-4), 11-29.
743 Beven, K., & Lane, S. (2019). Invalidation of Models and Fitness-for-Purpose: A Rejectionist Approach. In
744 C. Beisbart & N. J. Saam (Eds.), *Computer Simulation Validation: Fundamental Concepts,*
745 *Methodological Frameworks, and Philosophical Perspectives* (pp. 145-171). Cham: Springer
746 International Publishing.
747 Brandt, M. (1990). Simulation of Runoff and Nitrate Transport from Mixed Basins in Sweden. *Nordic*
748 *Hydrology, 21*(1), 13-34. <Go to ISI>://WOS:A1990DC94500002
749 Clow, D. W., & Mast, M. A. (2010). Mechanisms for chemostatic behavior in catchments: Implications for
750 CO2 consumption by mineral weathering. *Chemical Geology, 269*(1-2), 40-51. <Go to
751 ISI>://WOS:000274869700006
752 Davidson, E. A., Ishida, F. Y., & Nepstad, D. C. (2004). Effects of an experimental drought on soil
753 emissions of carbon dioxide, methane, nitrous oxide, and nitric oxide in a moist tropical forest.
754 *Glob. Chang. Biol., 10*(5), 718-730.
755 https://onlinelibrary.wiley.com/doi/pdfdirect/10.1111/j.1365-
756 2486.2004.00762.x?download=true

757 http://dx.doi.org/10.1111/j.1365-2486.2004.00762.x
758 Davidson, E. A., & Janssens, I. A. (2006). Temperature sensitivity of soil carbon decomposition and
759 feedbacks to climate change. *Nature, 440*(7081), 165-173. <Go to ISI>://WOS:000235839500036
760 Dean, J. F. (2019). Groundwater Dependent Ecosystems in Arid Zones Can Use Ancient Subterranean
761 Carbon as an Energy Source in the Local Food Web. *Journal of Geophysical Research-*
762 *Biogeosciences, 124*(4), 733-736. <Go to ISI>://WOS:000469076200001
763 Elberling, B. (2005). Temperature and oxygen control on pyrite oxidation in frozen mine tailings. *Cold*
764 *Regions Science and Technology, 41*(2), 121-133. <Go to ISI>://WOS:000227209200004

765 Fatichi, S., Vivoni, E. R., Ogden, F. L., Ivanov, V. Y., Mirus, B., Gochis, D., et al. (2016). An overview of
766 current applications, challenges, and future trends in distributed process-based models in
767 hydrology. *J. Hydrol., 537*, 45-60.
768 http://www.sciencedirect.com/science/article/pii/S0022169416301317

769 https://ac.els-cdn.com/S0022169416301317/1-s2.0-S0022169416301317-main.pdf?_tid=edb0408c-
770 df25-4ba2-8cf4-a989015274aa&acdnat=1532501836_5ac450b5f696bbf028432dafe05640c8

771 http://dx.doi.org/10.1016/j.jhydrol.2016.03.026
772 Filoso, S., Vallino, J., Hopkinson, C., Rastetter, E., & Claessens, L. (2004). Modeling nitrogen transport in
773 the Ipswich River Basin, Massachusetts, using a hydrological simulation program in fortran
774 (HSPF). *Journal of the American Water Resources Association, 40*(5), 1365-1384. <Go to
775 ISI>://WOS:000224721900019
776 Frisbee, M. D., Wilson, J. L., Gomez-Velez, J. D., Phillips, F. M., & Campbell, A. R. (2013). Are we missing
777 the tail (and the tale) of residence time distributions in watersheds? *Geophysical Research*
778 *Letters, 40*(17), 4633-4637. https://agupubs.onlinelibrary.wiley.com/doi/abs/10.1002/grl.50895

779 https://agupubs.onlinelibrary.wiley.com/doi/pdfdirect/10.1002/grl.50895?download=true
780 Helgeson, H. C., Murphy, W. M., & Aagaard, P. (1984). Thermodynamic and Kinetic Constraints on
781 Reaction-Rates among Minerals and Aqueous-Solutions .2. Rate Constants, Effective Surface-
782 Area, and the Hydrolysis of Feldspar. *Geochimica Et Cosmochimica Acta, 48*(12), 2405-2432. <Go
783 to ISI>://WOS:A1984TY25900001
784 Hindmarsh, A. C., Brown, P. N., Grant, K. E., Lee, S. L., Serban, R., Shumaker, D. E., & Woodward, C. S.
785 (2005). SUNDIALS: Suite of nonlinear and differential/algebraic equation solvers. *Acm*
786 *Transactions on Mathematical Software, 31*(3), 363-396. <Go to ISI>://WOS:000232597800006
787 Höge, M., Wöhling, T., & Nowak, W. (2018). A Primer for Model Selection: The Decisive Role of Model
788 Complexity. *Water Resources Research, 54*(3), 1688-1715. <Go to ISI>://WOS:000430364900016
789 Hou, C. Y., Chu, M. L., Botero-Acosta, A., & Guzman, J. A. (2021). Modeling field scale nitrogen non-point
790 source pollution (NPS) fate and transport: Influences from land management practices and
791 climate. *Science of the Total Environment, 759*. <Go to ISI>://WOS:000605764100059
792 Hu, X., McIsaac, G. E., David, M. B., & Louwers, C. A. L. (2007). Modeling riverine nitrate export from an
793 East-Central Illinois watershed using SWAT. *Journal of Environmental Quality, 36*(4), 996-1005.
794 <Go to ISI>://WOS:000247941900008
795 Husic, A., Fox, J., Adams, E., Ford, W., Agouridis, C., Currens, J., & Backus, J. (2019). Nitrate Pathways,
796 Processes, and Timing in an Agricultural Karst System: Development and Application of a
797 Numerical Model. *Water Resour. Res., 55*(3), 2079-2103.
798 https://agupubs.onlinelibrary.wiley.com/doi/abs/10.1029/2018WR023703

799 https://agupubs.onlinelibrary.wiley.com/doi/pdfdirect/10.1029/2018WR023703?download=true

800 http://dx.doi.org/10.1029/2018wr023703
801 Jaber, F. H., & Shukla, S. (2012). Mike She: Model Use, Calibration, and Validation. *Transactions of the*
802 *Asabe, 55*(4), 1479-1489. <Go to ISI>://WOS:000309089900028
803 Jan, A., Coon, E. T., & Painter, S. L. (2021). Toward more mechanistic representations of biogeochemical
804 processes in river networks: Implementation and demonstration of a multiscale model.
805 *Environmental Modelling & Software, 145*, 105166.
806 https://www.sciencedirect.com/science/article/pii/S1364815221002097
807 Kendall, K. A., Shanley, J. B., & McDonnell, J. J. (1999). A hydrometric and geochemical approach to test
808 the transmissivity feedback hypothesis during snowmelt. *Journal of Hydrology, 219*(3-4), 188-
809 205.

Kirchner, J. W., Hooper, R. P., Kendall, C., Neal, C., & Leavesley, G. (1996). Testing and validating environmental models. *Science of the Total Environment, 183*(1-2), 33-47.

Laroche, A. M., Gallichand, J., Lagace, R., & Pesant, A. (1996). Simulating atrazine transport with HSPF in an agricultural watershed. *Journal of Environmental Engineering-Asce, 122*(7), 622-630. <Go to ISI>://WOS:A1996UU67100011

Lasaga, A. C. (1984). Chemical-Kinetics of Water-Rock Interactions. *Journal of Geophysical Research, 89*(Nb6), 4009-4025. <Go to ISI>://WOS:A1984TA45700003

Li, L. (2019). Watershed reactive transport. In J. Druhan & C. Tournassat (Eds.), *Reviews in Mineralogy & Geochemistry: REACTIVE TRANSPORT IN NATURAL AND ENGINEERED SYSTEMS* (Vol. 85): Mineralogical Society of America.

Li, L., Bao, C., Sullivan, P. L., Brantley, S., Shi, Y., & Duffy, C. (2017). Understanding watershed hydrogeochemistry: 2. Synchronized hydrological and geochemical processes drive stream chemostatic behavior. *Water Resources Research, 53*(3), 2346-2367.

Li, L., Maher, K., Navarre-Sitchler, A., Druhan, J., Meile, C., Lawrence, C., et al. (2017). Expanding the role of reactive transport models in critical zone processes. *Earth-Science Reviews, 165*, 280-301. <Go to ISI>://WOS:000394395800012

Li, L., Stewart, B., Zhi, W., Sadayappan, K., Ramesh, S., Kerins, D., et al. (2022). Climate Controls on River Chemistry. *Earths Future, 10*(6). <Go to ISI>://WOS:000809677300001

Li, L., Sullivan, P. L., Benettin, P., Cirpka, O. A., Bishop, K., Brantley, S. L., et al. (2021). Toward catchment hydro-biogeochemical theories. *Wiley Interdisciplinary Reviews-Water, 8*(1). <Go to ISI>://WOS:000595274300001

Lichtner, P. C. (1988). The Quasi-Stationary State Approximation to Coupled Mass-Transport and Fluid-Rock Interaction in a Porous-Medium. *Geochimica Et Cosmochimica Acta, 52*(1), 143-165. <Go to ISI>://WOS:A1988M048000013

Lindström, G., Johansson, B., Persson, M., Gardelin, M., & Bergström, S. (1997). Development and test of the distributed HBV-96 hydrological model. *Journal of Hydrology, 201*(1-4), 272-288. <Go to ISI>://WOS:000071296200014

Lindström, G., Pers, C., Rosberg, J., Stromqvist, J., & Arheimer, B. (2010). Development and testing of the HYPE (Hydrological Predictions for the Environment) water quality model for different spatial scales. *Hydrology Research, 41*(3-4), 295-319. <Go to ISI>://WOS:000279499700011

Lindström, G., & Rodhe, A. (1986). Modeling Water Exchange and Transit Times in Till Basins Using O-18. *Nordic Hydrology, 17*(4-5), 325-334. <Go to ISI>://WOS:A1986G406300011

Luo, Y. Z., & Zhang, M. H. (2009). Management-oriented sensitivity analysis for pesticide transport in watershed-scale water quality modeling using SWAT. *Environmental Pollution, 157*(12), 3370-3378. <Go to ISI>://WOS:000272334500026

Ma, L., Zhu, G. F., Chen, B. L., Zhang, K., Niu, S. L., Wang, J. S., et al. (2022). A globally robust relationship between water table decline, subsidence rate, and carbon release from peatlands. *Communications Earth & Environment, 3*(1). <Go to ISI>://WOS:000876332000003

Ma, Z. W., Guan, K. Y., Peng, B., Sivapalan, M., Li, L., Pan, M., et al. (2023). Agricultural nitrate export patterns shaped by crop rotation and tile drainage. *Water Research, 229*. <Go to ISI>://WOS:000923266100001

Macpherson, G. L., & Sullivan, P. L. (2019). Dust, impure calcite, and phytoliths: Modeled alternative sources of chemical weathering solutes in shallow groundwater. *Chemical Geology, 527*.

McDowell, N. G., Anderson-Teixeira, K., Biederman, J. A., Breshears, D. D., Fang, Y. L., Fernández-de-Uña, L., et al. (2023). Ecohydrological decoupling under changing disturbances and climate. *One Earth, 6*(3), 251-266. <Go to ISI>://WOS:000990186300001

Monod, J. (1949). The Growth of Bacterial Cultures. *Annual Review of Microbiology, 3*, 371-394. <Go to ISI>://WOS:A1949XS94800016

858 Neff, J. C., & Asner, G. P. (2001). Dissolved organic carbon in terrestrial ecosystems: synthesis and a
859 model. *Ecosystems, 4*, 29-48.
860 Or, D., Smets, B. F., Wraith, J. M., Dechesne, A., & Friedman, S. P. (2007). Physical constraints affecting
861 bacterial habitats and activity in unsaturated porous media - a review. *Advances in Water*
862 *Resources, 30*(6-7), 1505-1527. <Go to ISI>://WOS:000246902300009
863 Ottoy, S., Elsen, A., Van De Vreken, P., Gobin, A., Merckx, R., Hermy, M., & Van Orshoven, J. (2016). An
864 exponential change decline function to estimate soil organic carbon stocks and their changes
865 from topsoil measurements. *European Journal of Soil Science, 67*(6), 816-826. <Go to
866 ISI>://WOS:000388477100010
867 Pers, C., Temnerud, J., & Lindström, G. (2016). Modelling water, nutrients, and organic carbon in
868 forested catchments: a HYPE application. *Hydrological Processes, 30*(18), 3252-3273. <Go to
869 ISI>://WOS:000383466900011
870 Pettersson, A., Arheimer, B., & Johansson, B. (2001). Nitrogen concentrations simulated with HBV-N:
871 New response function and calibration strategy - Paper presented at the Nordic Hydrological
872 Conference (Uppsala, Sweden June, 2000). *Nordic Hydrology, 32*(3), 227-248. <Go to
873 ISI>://WOS:000171692200005
874 Porter, V. M., Shanley, J. B., Sebestyen, S. D., & Liu, F. (2022). Controls on decadal, annual, and seasonal
875 concentration-discharge relationships in the Sleepers River Research Watershed , Vermont,
876 northeastern United States. *Hydrol. Process., 36*(3). http://dx.doi.org/10.1002/hyp.14559
877 Rajib, A., Kim, I. L., Golden, H. E., Lane, C. R., Kumar, S. V., Yu, Z. Q., & Jeyalakshmi, S. (2020). Watershed
878 Modeling with Remotely Sensed Big Data: MODIS Leaf Area Index Improves Hydrology and
879 Water Quality Predictions. *Remote Sensing, 12*(13). <Go to ISI>://WOS:000555590800001
880 Sadayappan, K., Keen, R. M., Jarecke, K. M., Moreno, V., Nippert, J. B., Kirk, M. F., et al. (2023). Drier
881 streams despite a wetter climate in woody-encroached grasslands. *Journal of Hydrology*,
882 130388.
883 Sadayappan, K., Kerins, D., Shen, C. P., & Li, L. (2022). Nitrate concentrations predominantly driven by
884 human, climate, and soil properties in US rivers. *Water Research, 226*. <Go to
885 ISI>://WOS:000884794600004
886 Schlesinger, W. H., & Bernhardt, E. S. (2020). *Biogeochemistry: An Analysis of Global Change*
887 (4th ed.): Academic Press.
888 Sebestyen, S. D., Boyer, E. W., & Shanley, J. B. (2009). Responses of stream nitrate and DOC loadings to
889 hydrological forcing and climate change in an upland forest of the northeastern United States.
890 *Journal of Geophysical Research: Biogeosciences, 114*(G2), n/a-n/a.
891 Sebestyen, S. D., Boyer, E. W., Shanley, J. B., Kendall, C., Doctor, D. H., Aiken, G. R., & Ohte, N. (2008).
892 Sources, transformations, and hydrological processes that control stream nitrate and dissolved
893 organic matter concentrations during snowmelt in an upland forest. *Water Resources Research,*
894 *44*(12).
895 Seibert, J. (2000). Multi-criteria calibration of a conceptual runoff model using a genetic algorithm.
896 *Hydrology and Earth System Sciences, 4*(2), 215-224. <Go to ISI>://WOS:000090061500003
897 Seibert, J. (2005). HBV light version 2, user's manual. *Department of Earth Sciences, Uppsala University,*
898 *Uppsala*.
899 Seibert, J., & Bergström, S. (2022). A retrospective on hydrological catchment modelling based on half a
900 century with the HBV model. *Hydrol. Earth Syst. Sci., 26*(5), 1371-1388.
901 https://hess.copernicus.org/articles/26/1371/2022/
902 http://dx.doi.org/10.5194/hess-26-1371-2022

Seibert, J., Grabs, T., Kohler, S., Laudon, H., Winterdahl, M., & Bishop, K. (2009). Linking soil- and stream-water chemistry based on a Riparian Flow-Concentration Integration Model. *Hydrology and Earth System Sciences, 13*(12), 2287-2297. <Go to ISI>://WOS:000273059900002

Seibert, J., & Vis, M. J. P. (2012). Teaching hydrological modeling with a user-friendly catchment-runoff-model software package. *Hydrology and Earth System Sciences, 16*(9), 3315-3325. <Go to ISI>://WOS:000310475400019

Shanley, J. B. (2000). *Sleepers River, Vermont: A Water, Energy, and Biogeochemical Budgets Program Site* (Fact Sheet-166-99). Retrieved from

Shanley, J. B., Kendall, C., Smith, T. E., Wolock, D. M., & McDonnell, J. J. (2002). Controls on old and new water contributions to stream flow at some nested catchments in Vermont, USA. *Hydrological Processes, 16*(3), 589-609.

Shanley, J. B., Krám, P., Hruška, J., & Bullen, T. D. (2004). A Biogeochemical Comparison of Two Well-Buffered Catchments with Contrasting Histories of Acid Deposition. *Water, Air, & Soil Pollution: Focus, 4*(2/3), 325-342.

Shanley, J. B., Sebestyen, S. D., McDonnell, J. J., McGlynn, B. L., & Dunne, T. (2015). Water's Way at Sleepers River watershed - revisiting flow generation in a post-glacial landscape, Vermont USA. *Hydrological Processes, 29*(16), 3447-3459.

Soulet, G., Hilton, R. G., Garnett, M. H., Dellinger, M., Croissant, T., Ogric, M., & Klotz, S. (2018). Technical note: In situ measurement of flux and isotopic composition of CO2 released during oxidative weathering of sedimentary rocks. *Biogeosciences, 15*(13), 4087-4102. <Go to ISI>://WOS:000437364000003

Souza, L. F. T., Hirmas, D. R., Sullivan, P. L., Reuman, D. C., Kirk, M. F., Li, L., et al. (2023). Root distributions, precipitation, and soil structure converge to govern soil organic carbon depth distributions. *Geoderma, 437*, 116569. https://www.sciencedirect.com/science/article/pii/S001670612300246X

http://dx.doi.org/10.1016/j.geoderma.2023.116569

Steefel, C. I. (2009). CrunchFlow. *Software for modeling multicomponent reactive flow and transport. User's manual*, 12-91.

Steefel, C. I., Appelo, C. A. J., Arora, B., Jacques, D., Kalbacher, T., Kolditz, O., et al. (2015). Reactive transport codes for subsurface environmental simulation. *Computational Geosciences, 19*(3), 445-478. https://doi.org/10.1007/s10596-014-9443-x

http://dx.doi.org/10.1007/s10596-014-9443-x

https://link.springer.com/article/10.1007/s10596-014-9443-x

Steefel, C. I., & MacQuarrie, K. T. B. (1996). Approaches to modeling of reactive transport in porous media. *Reactive Transport in Porous Media, 34*, 83-129. <Go to ISI>://WOS:A1996BG55B00002

Stewart, B., Shanley, J. B., Kirchner, J. W., Norris, D., Adler, T., Bristol, C., et al. (2022). Streams as mirrors: Reading subsurface water chemistry from stream chemistry. *Water Resources Research, 58*(1), e2021WR029931.

Sullivan, P. L., Billings, S. A., Hirmas, D., Li, L., Zhang, X., Ziegler, S., et al. (2022). Embracing the dynamic nature of soil structure: A paradigm illuminating the role of life in critical zones of the Anthropocene. *Earth-Science Reviews, 225*. <Go to ISI>://WOS:000849987100002

Sullivan, P. L., Hynek, S. A., Gu, X., Singha, K., White, T., West, N., et al. (2016). Oxidative dissolution under the channel leads geomorphological evolution at the Shale Hills catchment. *American Journal of Science, 316*(10), 981-1026. http://www.ajsonline.org/content/316/10/981.abstract

http://www.ajsonline.org/content/316/10/981.full.pdf

948 Torres, M. A., West, A. J., & Clark, K. E. (2015). Geomorphic regime modulates hydrologic control of
949 chemical weathering in the Andes–Amazon. *Geochimica Et Cosmochimica Acta, 166*, 105-128.
950 https://www.sciencedirect.com/science/article/pii/S0016703715003907
951 Tune, A. K., Druhan, J. L., Wang, J., Bennett, P. C., & Rempe, D. M. (2020). Carbon Dioxide Production in
952 Bedrock Beneath Soils Substantially Contributes to Forest Carbon Cycling. *Journal of Geophysical*
953 *Research-Biogeosciences, 125*(12). <Go to ISI>://WOS:000603282000019
954 Van Cappellen, P., & Gaillard, J. (1996). Biogeochemical dynamics in aquatic sediments. In P. C. Lichtner,
955 C. I. Steefel, & E. H. Oelkers (Eds.), *Reactive Transport in Porous Media* (Vol. 34). Washington,
956 D.C.: Mineralogical society of America.
957 Van Meter, K. J., Van Cappellen, P., & Basu, N. B. (2018). Legacy nitrogen may prevent achievement of
958 water quality goals in the Gulf of Mexico. *Science, 360*(6387), 427-+. <Go to
959 ISI>://WOS:000430949600040
960 Veinbergs, A., Lagzdins, A., Jansons, V., Abramenko, K., & Sudars, R. (2017). Discharge and Nitrogen
961 Transfer Modelling in the Berze River: A HYPE Setup and Calibration. *Environmental and Climate*
962 *Technologies, 19*(1), 51-64. <Go to ISI>://WOS:000408475100005
963 Vis, M., Knight, R., Pool, S., Wolfe, W., & Seibert, J. (2015). Model calibration criteria for estimating
964 ecological flow characteristics. *Water, 7*(5), 2358-2381.
965 Wade, A. J., Durand, P., Beaujouan, V., Wessel, W. W., Raat, K. J., Whitehead, P. G., et al. (2002). A
966 nitrogen model for European catchments: INCA, new model structure and equations. *Hydrology*
967 *and Earth System Sciences, 6*(3), 559-582. <Go to ISI>://WOS:000177534200023
968 Walter, A. L., Frind, E. O., Blowes, D. W., Ptacek, C. J., & Molson, J. W. (1994). Modeling of
969 Multicomponent Reactive Transport in Groundwater .1. Model Development and Evaluation.
970 *Water Resources Research, 30*(11), 3137-3148. <Go to ISI>://WOS:A1994PP21300025
971 Wen, H., Brantley, S. L., Davis, K. J., Duncan, J. M., & Li, L. (2021). The limits of homogenization: How and
972 how much can a simple model represent hydrological dynamics at the catchment scale? *Water*
973 *Resour. Res.*
974 Wen, H., Perdrial, J., Abbott, B. W., Bernal, S., Dupas, R., Godsey, S. E., et al. (2020). Temperature
975 controls production but hydrology regulates export of dissolved organic carbon at the
976 catchment scale. *Hydrol. Earth Syst. Sci., 24*(2), 945-966. https://www.hydrol-earth-syst-
977 sci.net/24/945/2020/

978 https://www.hydrol-earth-syst-sci.net/24/945/2020/hess-24-945-2020.pdf

979 http://dx.doi.org/10.5194/hess-24-945-2020
980 Xiao, D., Brantley, S. L., & Li, L. (2021). Vertical connectivity regulates water transit time and chemical
981 weathering at the hillslope scale. *Water Resour. Res.*
982 https://agupubs.onlinelibrary.wiley.com/doi/abs/10.1029/2020WR029207

983 https://scholar.google.ca/scholar?cluster=15576254807719459705&hl=en&as_sdt=0,5&sciodt=0,5
984 Yan, Z. F., Bond-Lamberty, B., Todd-Brown, K. E., Bailey, V. L., Li, S. L., Liu, C. Q., & Liu, C. X. (2018). A
985 moisture function of soil heterotrophic respiration that incorporates microscale processes.
986 *Nature Communications, 9*. <Go to ISI>://WOS:000436958500009
987 Zamanian, K., Pustovoytov, K., & Kuzyakov, Y. (2016). Pedogenic carbonates: Forms and formation
988 processes. *Earth-Science Reviews, 157*, 1-17.
989 Zhi, W., & Li, L. (2020). The Shallow and Deep Hypothesis: Subsurface Vertical Chemical Contrasts Shape
990 Nitrate Export Patterns from Different Land Uses. *Environmental Science & Technology, 54*(19),
991 11915-11928. <Go to ISI>://WOS:000580444600030

992 Zhi, W., Shi, Y. N., Wen, H., Saberi, L., Ng, G. H. C., Sadayappan, K., et al. (2022). BioRT-Flux-PIHM v1.0: a
993 biogeochemical reactive transport model at the watershed scale. *Geoscientific Model*
994 *Development, 15*(1), 315-333. <Go to ISI>://WOS:000746474900001

995

Figure 1.

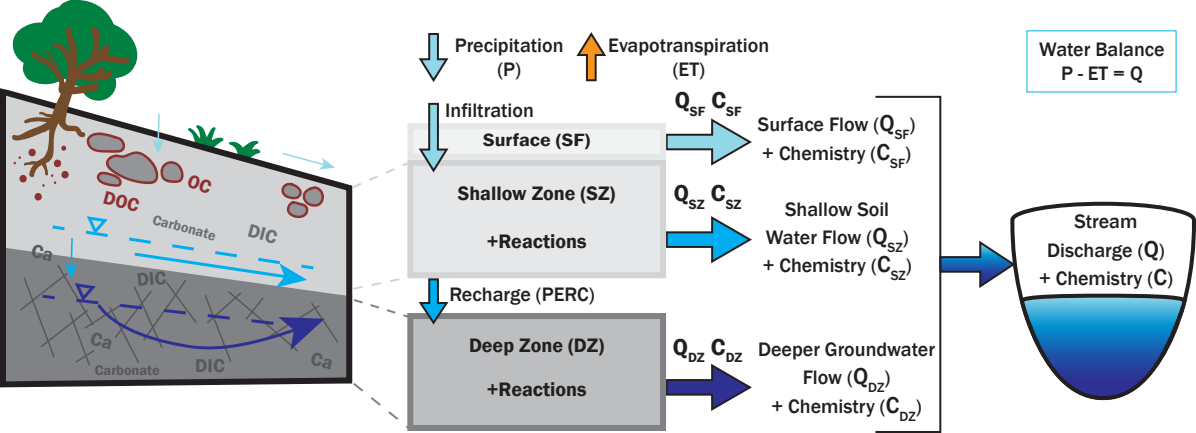
Precipitation (P)
Evapotranspiration (ET)
Water Balance P - ET = Q
Infiltration
Surface (SF)
Shallow Zone (SZ)
+Reactions
Recharge (PERC)
Deep Zone (DZ)
+Reactions
Q_{SF} C_{SF}
Surface Flow (Q_{SF}) + Chemistry (C_{SF})
Q_{SZ} C_{SZ}
Shallow Soil Water Flow (Q_{SZ}) + Chemistry (C_{SZ})
Q_{DZ} C_{DZ}
Deeper Groundwater Flow (Q_{DZ}) + Chemistry (C_{DZ})
Stream Discharge (Q) + Chemistry (C)
DOC
OC
Carbonate
DIC
Ca
DIC
Ca
Carbonate
DIC
Ca

Figure 2.

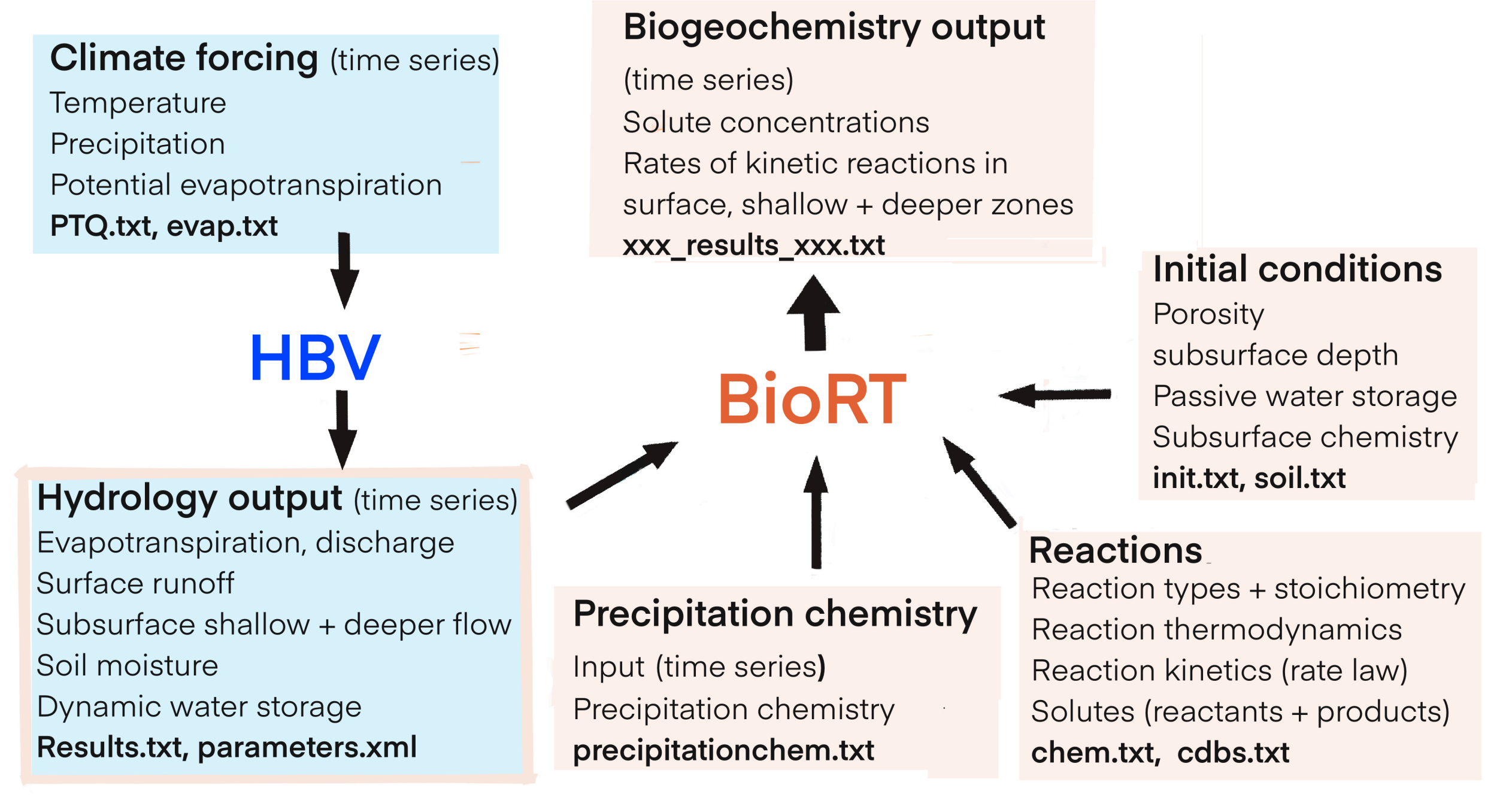
Climate forcing (time series)
Temperature
Precipitation
Potential evapotranspiration
PTQ.txt, evap.txt
HBV
Hydrology output (time series)
Evapotranspiration, discharge
Surface runoff
Subsurface shallow + deeper flow
Soil moisture
Dynamic water storage
Results.txt, parameters.xml
Biogeochemistry output
(time series)
Solute concentrations
Rates of kinetic reactions in
surface, shallow + deeper zones
xxx_results_xxx.txt
BioRT
Initial conditions
Porosity
subsurface depth
Passive water storage
Subsurface chemistry
init.txt, soil.txt
Precipitation chemistry
Input (time series)
Precipitation chemistry
precipitationchem.txt
Reactions
Reaction types + stoichiometry
Reaction thermodynamics
Reaction kinetics (rate law)
Solutes (reactants + products)
chem.txt, cdbs.txt

Figure 3.

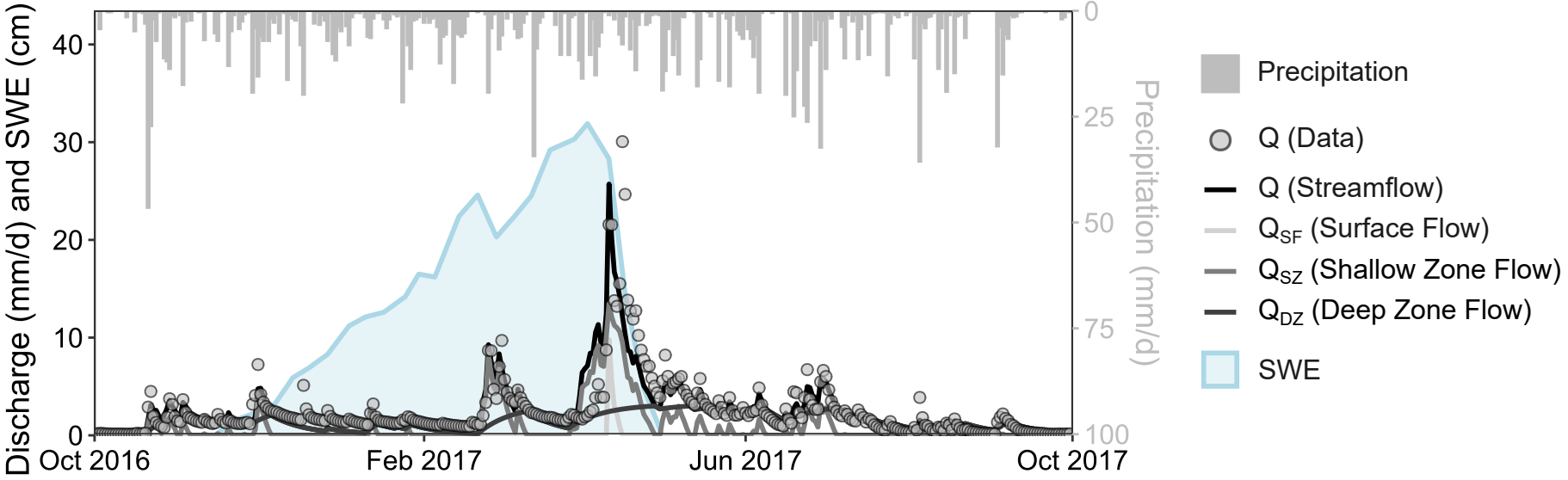
Discharge (mm/d) and SWE (cm)
40
30
20
10
0
Oct 2016
Feb 2017
Jun 2017
Oct 2017
0
25
50
75
100
Precipitation (mm/d)
Precipitation
Q (Data)
Q (Streamflow)
Q_{SF} (Surface Flow)
Q_{SZ} (Shallow Zone Flow)
Q_{DZ} (Deep Zone Flow)
SWE

Figure 4.

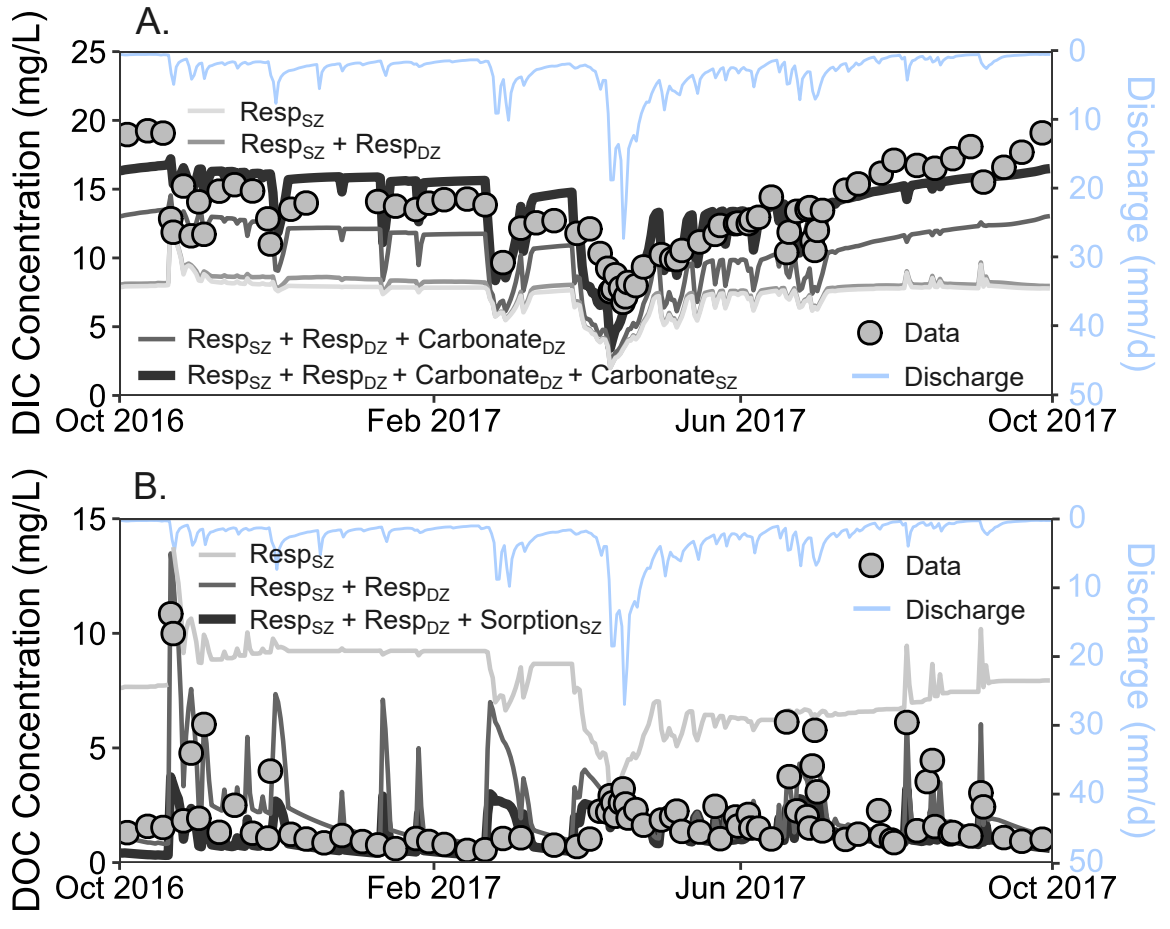
A.
DIC Concentration (mg/L)
Discharge (mm/d)
Resp$_{SZ}$
Resp$_{SZ}$ + Resp$_{DZ}$
Resp$_{SZ}$ + Resp$_{DZ}$ + Carbonate$_{DZ}$
Resp$_{SZ}$ + Resp$_{DZ}$ + Carbonate$_{DZ}$ + Carbonate$_{SZ}$
Data
Discharge
Oct 2016
Feb 2017
Jun 2017
Oct 2017
B.
DOC Concentration (mg/L)
Discharge (mm/d)
Resp$_{SZ}$
Resp$_{SZ}$ + Resp$_{DZ}$
Resp$_{SZ}$ + Resp$_{DZ}$ + Sorption$_{SZ}$
Data
Discharge
Oct 2016
Feb 2017
Jun 2017
Oct 2017

Figure 5.

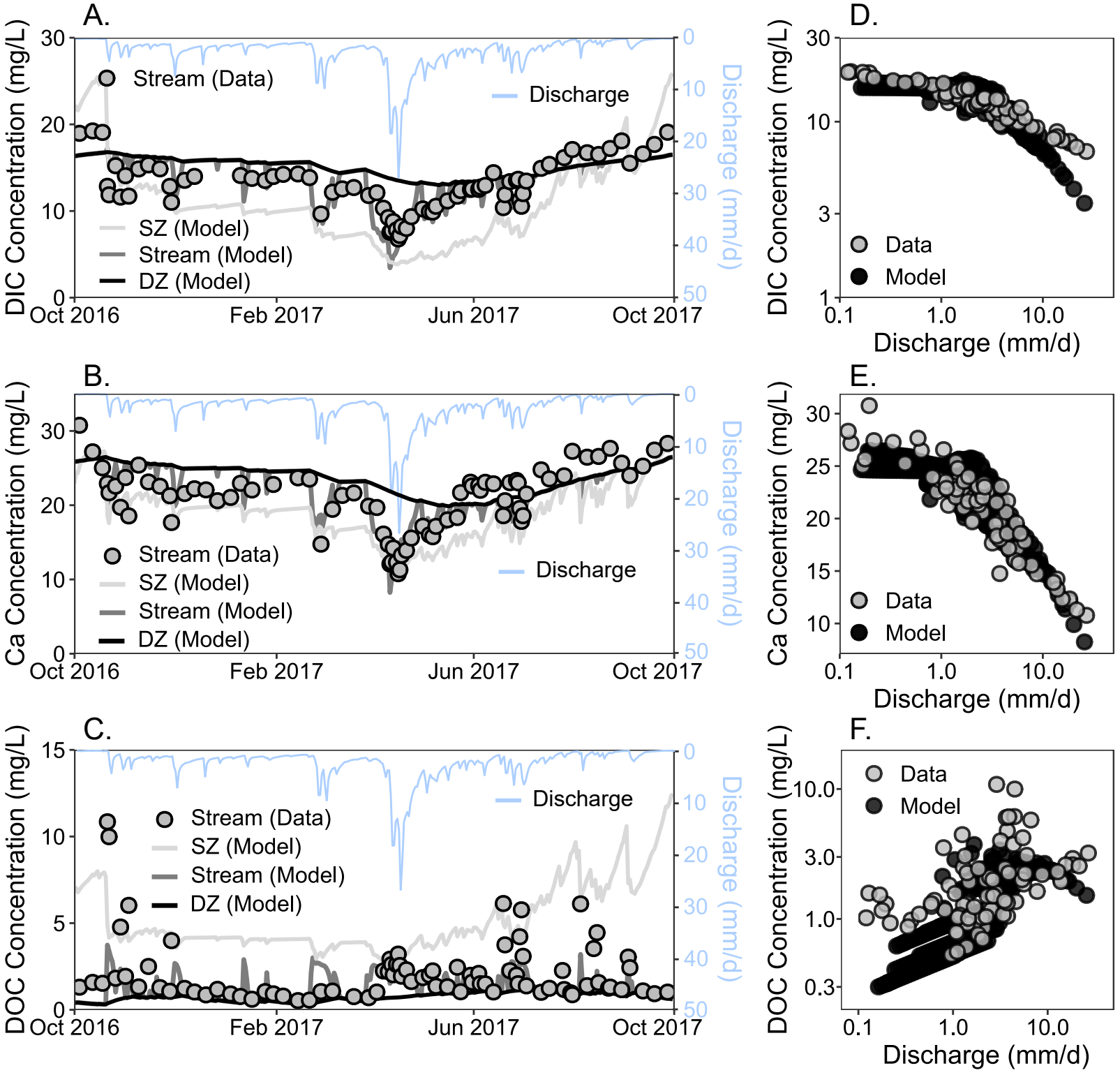
A.
DIC Concentration (mg/L)
Discharge (mm/d)
Stream (Data)
Discharge
SZ (Model)
Stream (Model)
DZ (Model)
Oct 2016
Feb 2017
Jun 2017
Oct 2017
B.
Ca Concentration (mg/L)
Discharge (mm/d)
Stream (Data)
SZ (Model)
Stream (Model)
DZ (Model)
Discharge
Oct 2016
Feb 2017
Jun 2017
Oct 2017
C.
DOC Concentration (mg/L)
Discharge (mm/d)
Stream (Data)
SZ (Model)
Stream (Model)
DZ (Model)
Discharge
Oct 2016
Feb 2017
Jun 2017
Oct 2017
D.
DIC Concentration (mg/L)
Data
Model
Discharge (mm/d)
E.
Ca Concentration (mg/L)
Data
Model
Discharge (mm/d)
F.
DOC Concentration (mg/L)
Data
Model
Discharge (mm/d)

Figure 6.

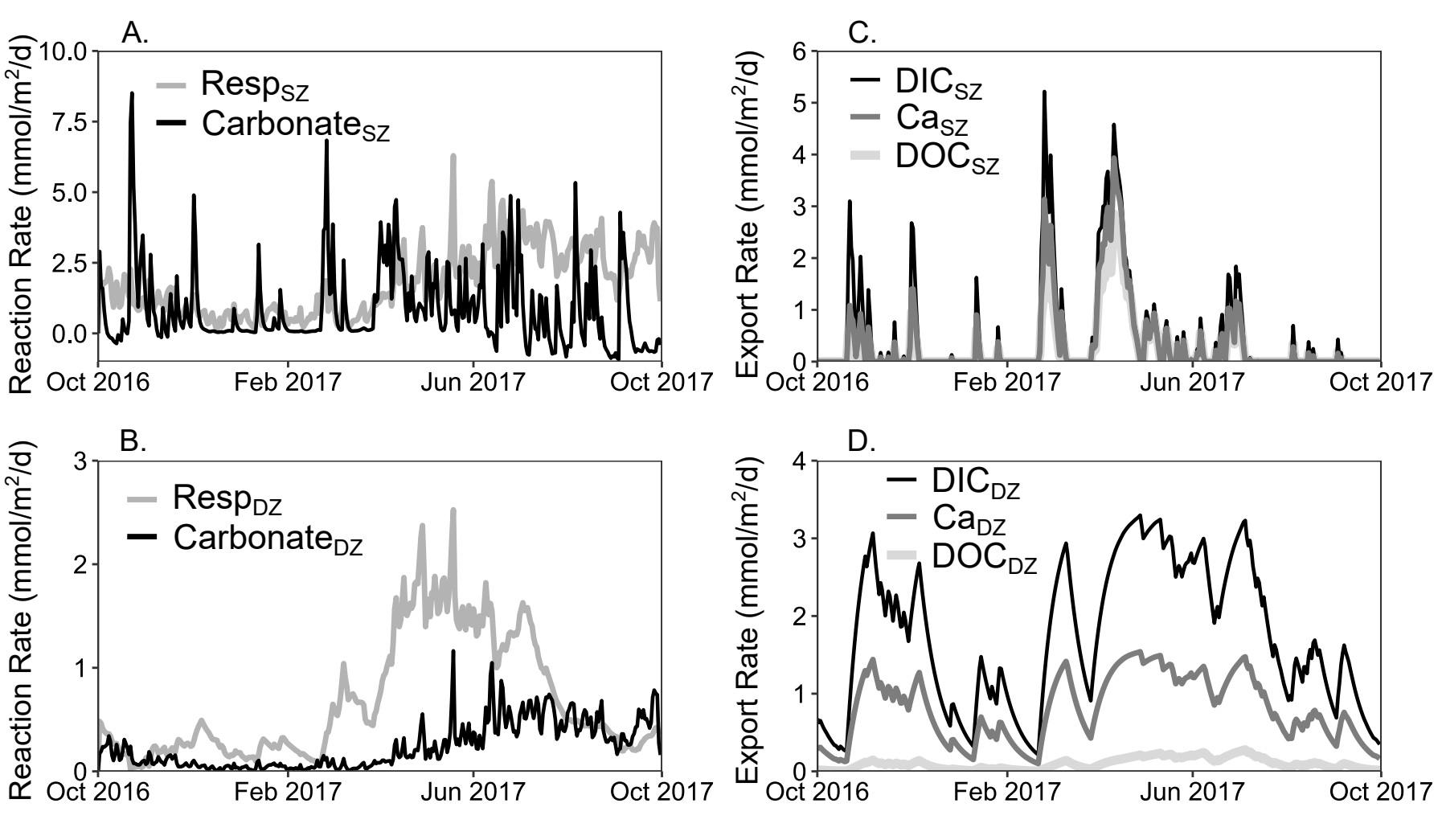
A.
Reaction Rate (mmol/m2/d)
10.0
7.5
5.0
2.5
0.0
Resp$_{SZ}$
Carbonate$_{SZ}$
Oct 2016
Feb 2017
Jun 2017
Oct 2017
C.
Export Rate (mmol/m2/d)
6
5
4
3
2
1
0
DIC$_{SZ}$
Ca$_{SZ}$
DOC$_{SZ}$
Oct 2016
Feb 2017
Jun 2017
Oct 2017
B.
Reaction Rate (mmol/m2/d)
3
2
1
0
Resp$_{DZ}$
Carbonate$_{DZ}$
Oct 2016
Feb 2017
Jun 2017
Oct 2017
D.
Export Rate (mmol/m2/d)
4
3
2
1
0
DIC$_{DZ}$
Ca$_{DZ}$
DOC$_{DZ}$
Oct 2016
Feb 2017
Jun 2017
Oct 2017

Figure 7.

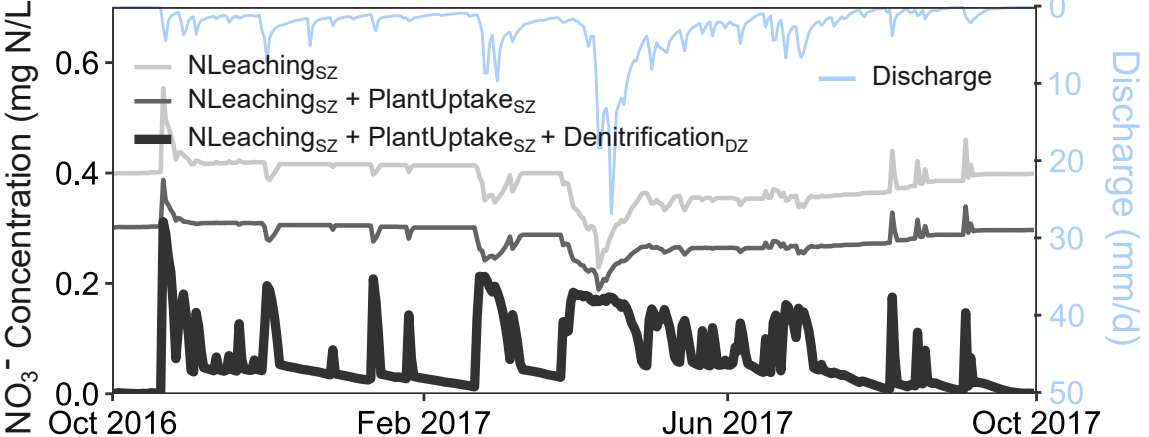
NO3- Concentration (mg N/L)
0.0
0.2
0.4
0.6
NLeachingSZ
NLeachingSZ + PlantUptakeSZ
NLeachingSZ + PlantUptakeSZ + DenitrificationDZ
Discharge
0
10
20
30
40
50
Discharge (mm/d)
Oct 2016
Feb 2017
Jun 2017
Oct 2017

Figure 8.

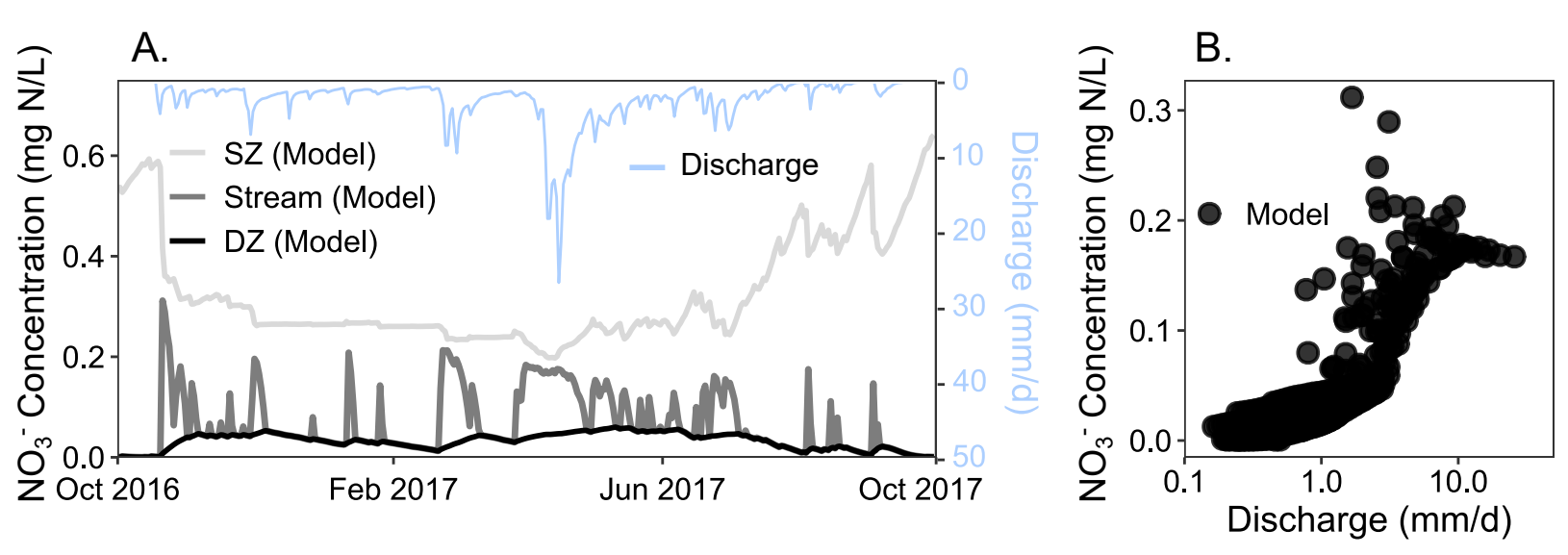
A.
B.
SZ (Model)
Stream (Model)
DZ (Model)
Discharge
Model
NO_3^- Concentration (mg N/L)
Discharge (mm/d)
0.0
0.2
0.4
0.6
0
10
20
30
40
50
0.1
0.2
0.3
1.0
10.0
Oct 2016
Feb 2017
Jun 2017
Oct 2017

Figure 9.

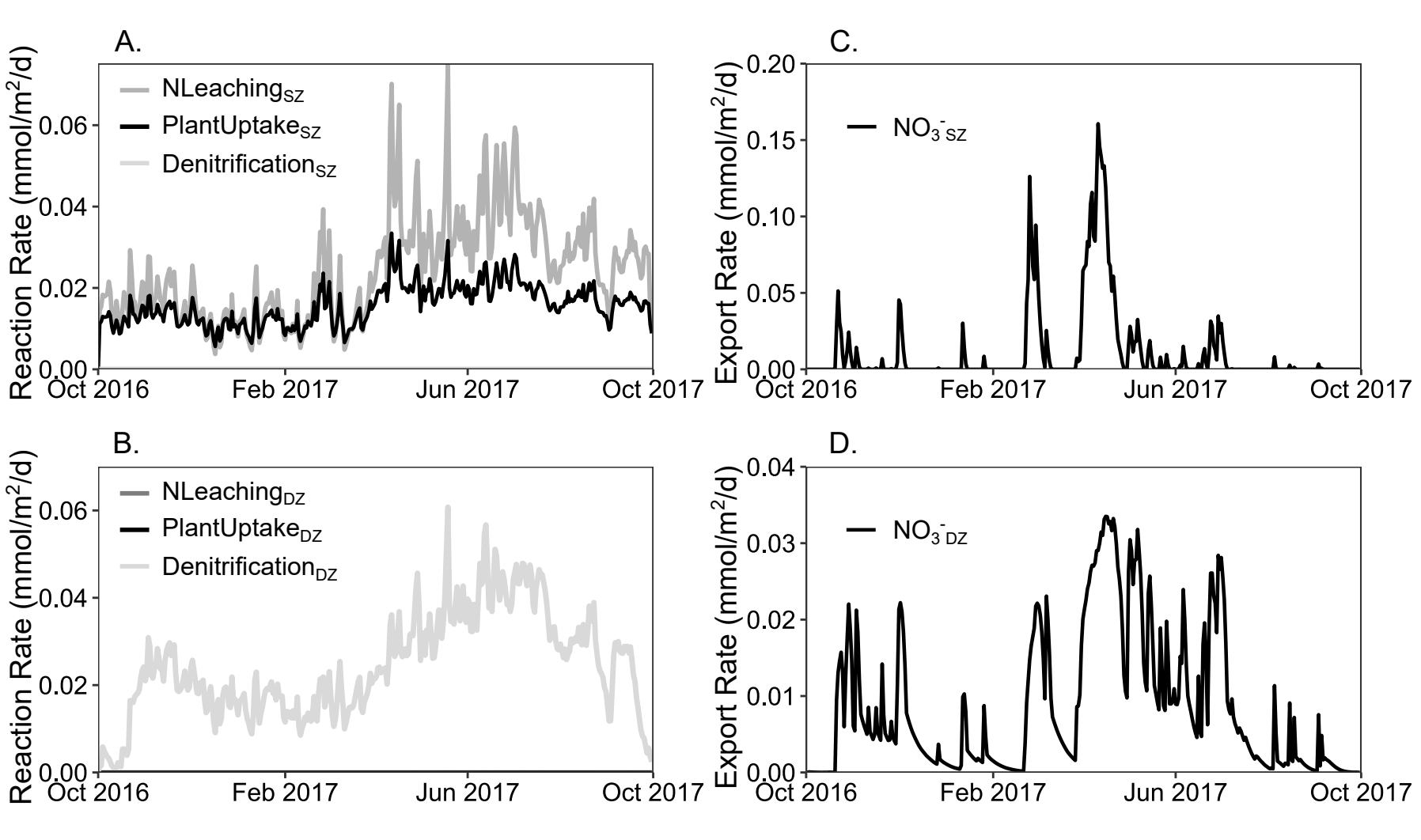
A.
NLeaching$_{SZ}$
PlantUptake$_{SZ}$
Denitrification$_{SZ}$
Reaction Rate (mmol/m^2/d)
0.00
0.02
0.04
0.06
Oct 2016
Feb 2017
Jun 2017
Oct 2017
C.
$NO_3^-{}_{SZ}$
Export Rate (mmol/m^2/d)
0.00
0.05
0.10
0.15
0.20
Oct 2016
Feb 2017
Jun 2017
Oct 2017
B.
NLeaching$_{DZ}$
PlantUptake$_{DZ}$
Denitrification$_{DZ}$
Reaction Rate (mmol/m^2/d)
0.00
0.02
0.04
0.06
Oct 2016
Feb 2017
Jun 2017
Oct 2017
D.
$NO_3^-{}_{DZ}$
Export Rate (mmol/m^2/d)
0.00
0.01
0.02
0.03
0.04
Oct 2016
Feb 2017
Jun 2017
Oct 2017